

## RESEARCH ARTICLE

# Claudin-4 is required for modulation of paracellular permeability by muscarinic acetylcholine receptor in epithelial cells

Xin Cong<sup>1,2</sup>, Yan Zhang<sup>1</sup>, Jing Li<sup>3</sup>, Mei Mei<sup>3</sup>, Chong Ding<sup>4</sup>, Ruo-Lan Xiang<sup>1</sup>, Li-Wei Zhang<sup>5</sup>, Yun Wang<sup>2</sup>, Li-Ling Wu<sup>1,\*</sup> and Guang-Yan Yu<sup>2,\*</sup>

**ABSTRACT**

The epithelial cholinergic system plays an important role in water, ion and solute transport. Previous studies have shown that activation of muscarinic acetylcholine receptors (mAChRs) regulates paracellular transport of epithelial cells; however, the underlying mechanism is still largely unknown. Here, we found that mAChR activation by carbachol and cevimeline reduced the transepithelial electrical resistance (TER) and increased the permeability of paracellular tracers in rat salivary epithelial SMG-C6 cells. Carbachol induced downregulation and redistribution of claudin-4, but not occludin or ZO-1 (also known as TJP1). Small hairpin RNA (shRNA)-mediated claudin-4 knockdown suppressed, whereas claudin-4 overexpression retained, the TER response to carbachol. Mechanistically, the mAChR-modulated claudin-4 properties and paracellular permeability were triggered by claudin-4 phosphorylation through ERK1/2 (also known as MAPK3 and MAPK1, respectively). Mutagenesis assay demonstrated that S195, but not S199, S203 or S207, of claudin-4, was the target for carbachol. Subsequently, the phosphorylated claudin-4 interacted with  $\beta$ -arrestin2 and triggered claudin-4 internalization through the clathrin-dependent pathway. The internalized claudin-4 was further degraded by ubiquitylation. Taken together, these findings suggested that claudin-4 is required for mAChR-modulated paracellular permeability of epithelial cells through an ERK1/2,  $\beta$ -arrestin2, clathrin and ubiquitin-dependent signaling pathway.

**KEY WORDS:** Tight junction, Claudin-4, Muscarinic acetylcholine receptor, Paracellular permeability

**INTRODUCTION**

Tight junctions are specialized structures located in the most apical region of lateral membranes between neighboring cells, establishing a barrier to the diffusion of solutes through paracellular pathway in polarized epithelia (Tsukita et al., 2001; González-Mariscal et al., 2003). Proteins comprising tight junctions include transmembrane proteins, such as claudins and occludin, together with intracellular

proteins, like ZO-1 (also known as TJP1). The tight junction transmembrane proteins associate laterally with those from other tight junctions in the apposing membranes of adjacent cells, forming the intracellular space that contributes to the sealing, and are indispensable for paracellular transport, whereas the intracellular proteins play an important role in the establishment and maintenance of tight junction structure owing to their ability to link transmembrane proteins with actin cytoskeleton (Krause et al., 2008; Schulzke et al., 2012). To date, an enormous amount of research has focused on the active and essential role of tight junctions in intestinal, renal, airway, mammary, salivary, dermal and bladder epithelial function (Coyne et al., 2002; Roxas et al., 2010; Yang et al., 2010; Peerapen and Thongboonkerd, 2011; Nagaoka et al., 2012; Wood et al., 2012).

Muscarinic acetylcholine receptors (mAChRs) are G-protein-coupled receptors (GPCRs), and include the M1–M5 subtypes (encoded by *Chrm1–Chrm5*). In epithelial cells, mAChR plays a crucial role in regulating water, ion and solute transport. For example, mAChR activation causes an elevated intracellular  $\text{Ca}^{2+}$ , which in turn causes the opening of  $\text{Cl}^-$  channels and the trafficking of aquaporins to form water pores, leading to increased secretion through the transcellular pathway in salivary epithelium (Ishikawa et al., 1998; Melvin et al., 2005). However, limited data are available on the effects of mAChR activation on the tight-junction-based paracellular pathway. In MDCK cells, the mAChR agonist carbachol inhibits the pertussis-toxin-induced decrease in paracellular permeability (Balda et al., 1991). In rat submandibular epithelium, carbachol or pilocarpine increases paracellular transport and causes morphological changes in tight junction structure (Segawa, 1994; Hashimoto et al., 2003). These observations suggest that mAChR activation might also regulate epithelial material transport through paracellular pathway. But, to date, how mAChR modulates tight junctions and thereby affects the paracellular barrier function is largely unknown.

Therefore, the present study was designed to explore the effects of mAChR activation on tight junction properties, together with the potential regulatory mechanism using the rat salivary epithelial SMG-C6 cell line. Our findings provide evidence for a new pathway whereby mAChR activation promotes paracellular transport by regulating the content and distribution of the tight junction transmembrane protein claudin-4.

**RESULTS**

## **mAChR activation decreases transepithelial electrical resistance and increases paracellular permeability**

To identify the direct effect of mAChR activation on epithelial paracellular permeability, SMG-C6 cells were cultured for 7 days on Transwell inserts to form a polarized monolayer. The basal transepithelial electrical resistance (TER) value of untreated

<sup>1</sup>Center for Salivary Gland Diseases of Peking University School and Hospital of Stomatology, Department of Physiology and Pathophysiology, School of Basic Medical Sciences, Peking University Health Science Center and Key Laboratory of Molecular Cardiovascular Sciences, Ministry of Education, Beijing Key Laboratory of Cardiovascular Receptors Research, Beijing 100191, China. <sup>2</sup>Neuroscience Research Institute and Department of Neurobiology, The Key Laboratory for Neuroscience of the Ministry of Education and Health, Peking University Health Science Center, Beijing 100191, China. <sup>3</sup>Department of Oral and Maxillofacial Surgery, Peking University School and Hospital of Stomatology, Beijing 100081, China. <sup>4</sup>Central Laboratory, Peking University School and Hospital of Stomatology, Beijing 100081, China. <sup>5</sup>Department of Oral Medicine and Traditional Chinese Medicine, Peking University School and Hospital of Stomatology, Beijing 100081, China.

\*Authors for correspondence (pathophy@bjmu.edu.cn; gyyu@263.net)

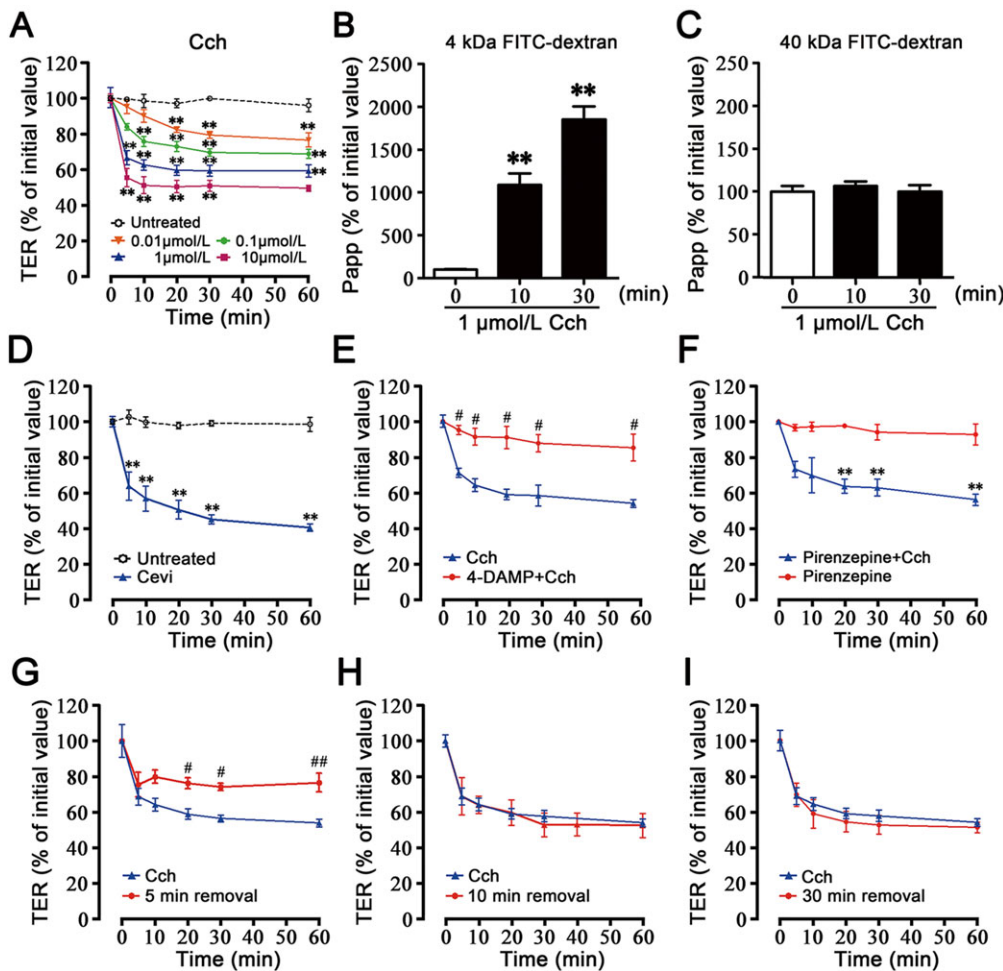


**Fig. 1. Activation of mAChR increases the paracellular permeability of SMG-C6 cells.**

(A) Transepithelial electrical resistance (TER) values were measured by an EVOM. Carbachol (Cch) induced TER decreases in a dose-dependent manner. (B) The apparent permeability coefficients ( $P_{app}$ ) for 4-kDa FITC-dextran was increased by 1  $\mu\text{mol/l}$  carbachol treatment for 10 and 30 min. (C) Carbachol did not affect the  $P_{app}$  for 40-kDa FITC-dextran. (D) 10  $\mu\text{mol/l}$  cevimeline (Cevi), an M3-specific selective agonist, caused significant TER decreases. (E) Pretreatment with the M3 antagonist 4-DAMP (10  $\mu\text{mol/l}$ ) significantly abolished the carbachol-induced TER decreases. (F) In the cells pretreated with the M1 antagonist pirenzepine (1  $\text{nmol/l}$ ), carbachol still induced significant TER decreases. (G) A partial recovery in TER was observed after carbachol removal at 5 min. (H,I) Carbachol removal at 10 and 30 min did not affect the carbachol-induced TER decreases. Values are mean  $\pm$  s.d. from three independent experiments performed in duplicate. \*\* $P < 0.01$  compared with the untreated cells. # $P < 0.05$ , ## $P < 0.01$  compared with the carbachol-treated cells.

monolayer was  $632.8 \pm 107.1 \Omega \text{ cm}^2$ , which represented a relatively ‘tight’ epithelium according to the description of electrical characteristics (Anderson and Van Itallie, 2009). After treatment with 0.01  $\mu\text{mol/l}$  carbachol, TER values slowly decreased and showed significant differences starting at 20 min compared with untreated cells, whereas 0.1  $\mu\text{mol/l}$  carbachol caused a significant TER decrease from 10 to 60 min. At 1 and 10  $\mu\text{mol/l}$ , the carbachol-induced responses were much earlier as shown by the rapid and prominent TER drops starting at 5 min (Fig. 1A). 1  $\mu\text{mol/l}$  of carbachol was used in the following experiments except when indicated. These data indicate that carbachol induces TER decreases in a dose-dependent manner.

The paracellular permeability is also evaluated by using FITC-dextran as a non-charged paracellular tracer. Results showed that the apparent permeability coefficients ( $P_{app}$ ) for 4-kDa FITC-dextran were greatly increased by carbachol, whereas the  $P_{app}$  for a larger FITC-dextran (40 kDa) was unaffected (Fig. 1B,C), indicating that the increase in paracellular permeability induced by carbachol mostly affects small macromolecules. These results provide more evidence that mAChR activation can directly increase the paracellular permeability of SMG-C6 cells.

We further detected the mAChR subtype that modulated paracellular permeability. Cevimeline (10  $\mu\text{mol/l}$ ), an M3-specific agonist, caused rapid and significant TER decreases, whereas pretreatment with 4-DAMP (10  $\mu\text{mol/l}$ ), an M3 selective antagonist, abolished the carbachol-induced TER decreases (Fig. 1D,E). By contrast, pretreatment with pirenzepine (1  $\text{nmol/l}$ ), an M1-specific

antagonist, did not affect this response (Fig. 1F), indicating that M3, but not M1, is the main subtype involved in the mAChR-modulated tight junction function in SMG-C6 cells.

We next detected TER responses to the removal of carbachol at different time points. Compared with the cells treated with carbachol constantly, a partial recovery in TER was observed at 5 min after the withdrawal (Fig. 1G). By contrast, withdrawal at 10 and 30 min did not affect the carbachol-induced TER decreases (Fig. 1H,I). The partially reversible and irreversible TER responses caused by carbachol suggests that mAChR activation probably modulates paracellular permeability by influencing the content and distribution of tight junction proteins.

#### mAChR activation reduces claudin-4 protein expression

We then examined the effect of mAChR activation on tight junction content in SMG-C6 cells. Carbachol significantly decreased the amount of claudin-4 protein in a dose- and time-dependent manner, whereas the expressions of other tight junction components, including occludin, claudin-1 and ZO-1, as well as adherens junction component E-cadherin, were unaffected (Fig. 2A,B). The mRNA levels of claudin-1, claudin-3, claudin-4, occludin and ZO-1, were unaffected by carbachol from 5 to 60 min and from 1 to 36 h (supplementary material Fig. S1A–J), suggesting that mAChR activation regulates claudin-4 expression at the protein level. We further extracted the membrane and cytoplasm fractions of carbachol-treated cells, and found that the intensities of claudin-4 protein were significantly decreased in the membrane from 5 to 60 min, whereas

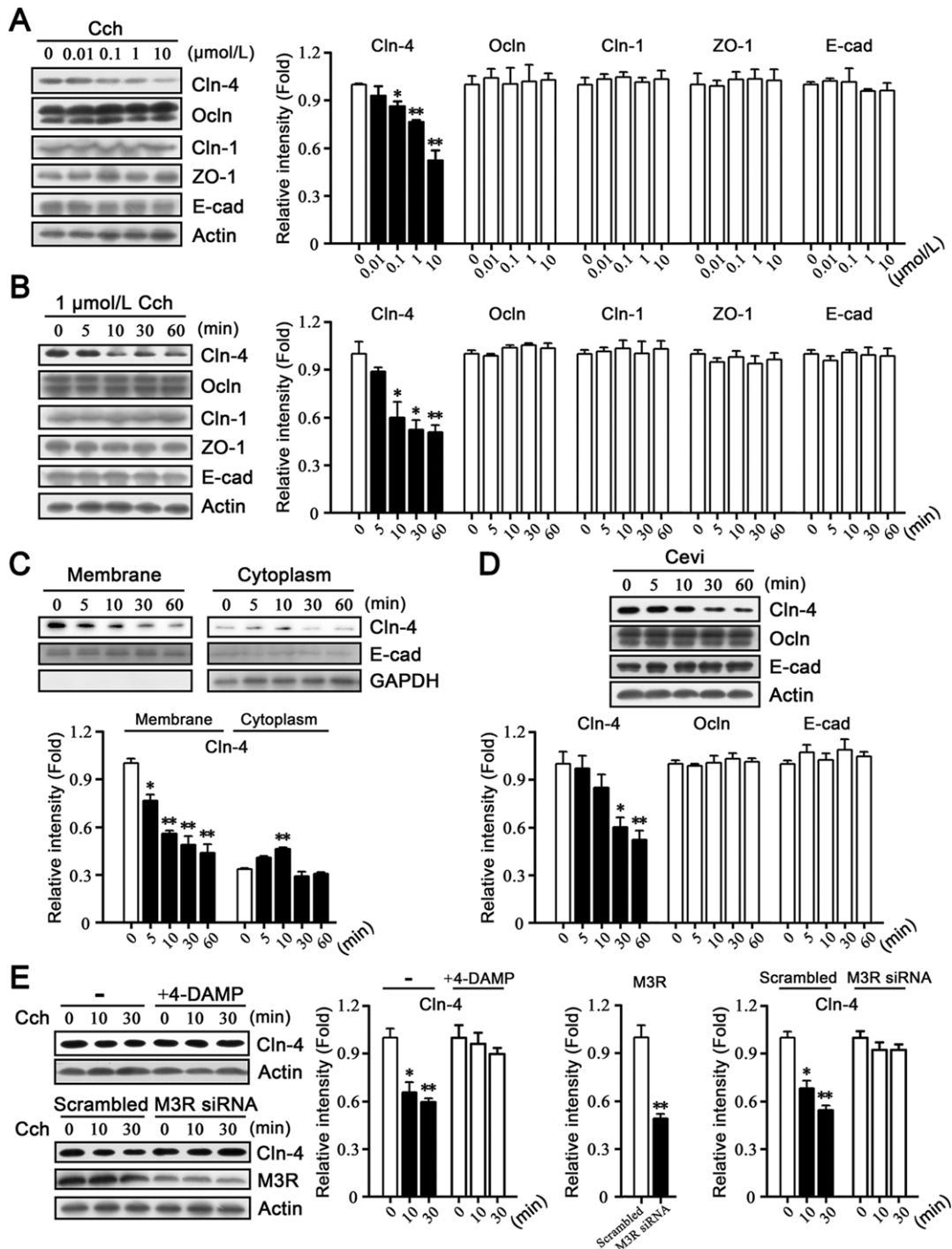


**Fig. 2. Activation of mAChR downregulates claudin-4 protein expression.** (A) The amounts of claudin-4 (Cln-4), occludin (Ocln), claudin-1 (Cln-1), ZO-1 and E-cadherin (E-cad) after carbachol (Cch) stimulation for 10 min were detected by western blotting (left). Statistical analysis showed that claudin-4 protein levels were significantly reduced by carbachol in a dose-dependent manner, whereas the other proteins were unaffected (right). (B) 1 μmol/l carbachol significantly decreased claudin-4 expression in a time-dependent manner, whereas the levels of the other proteins were unchanged (right). (C) Carbachol caused decreases in the amount of claudin-4 protein in the membrane fraction, together with a transient increase in the amount of claudin-4 protein in the cytoplasm fraction at 10 min, which returned to the baseline at 30 and 60 min. (D) 10 μmol/l cevimeline (Cevi) decreased claudin-4 levels, but not occludin or E-cadherin. (E) Pretreatment with 4-DAMP (10 μmol/l) or knockdown of M3 (M3R) by siRNA significantly abolished the carbachol-induced claudin-4 decreases. Values are mean±s.d. from three independent experiments performed in duplicate. \* $P < 0.05$  and \*\* $P < 0.01$  compared with the untreated cells.

transiently increased to a peak at 10 min in the cytoplasm and returned to baseline afterwards (Fig. 2C), indicating that carbachol causes a rapid trafficking of claudin-4 from the membrane into the cytoplasm. Note that statistical analysis showed that the extent of claudin-4 protein increase in the cytoplasm did not equalize the decrease in the

membrane amount, suggesting that carbachol-induced claudin-4 internalization accompanies claudin-4 degradation. The levels of E-cadherin, a membrane-enriched marker, were unchanged, and GAPDH served as an invariable cytoplasm control (Fig. 2C). Moreover, we performed the cell surface biotinylation assay to

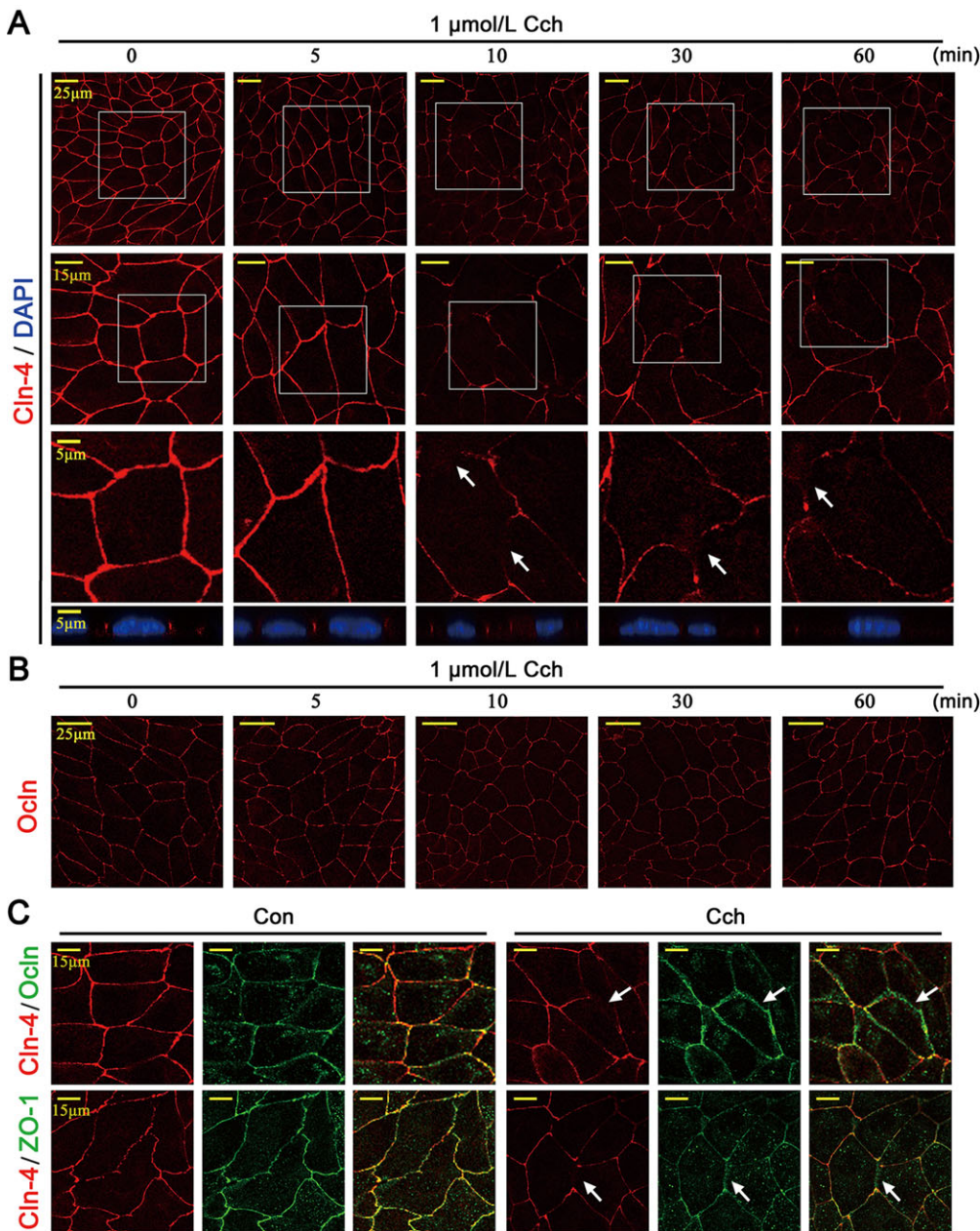


**Fig. 3. Carbachol alters the distribution of claudin-4.** (A) The continuous distribution of claudin-4 (Cln-4) in the cell borders was gradually diminished by carbachol (Cch) for 10 to 60 min. White arrows pointed to those regions where the apical claudin-4 staining were missing. *x-z* images show that the claudin-4-positive spots in the apical region between neighboring cells were disturbed by carbachol. Each image is a representative of three separate experiments in duplicate. *x-y* images are presented by lower and higher magnifications, and *x-z* images at higher magnifications. (B) The distribution of occludin (Ocln) was unaffected by carbachol. (C) Claudin-4 was co-stained with either occludin (upper panels) or ZO-1 (lower panels). Carbachol stimulation (10 min) altered the apical continuities of claudin-4, but not those of occludin or ZO-1 at the same sites (white arrows).

measure endocytosis of claudin-4. Carbachol caused significant decreases in the amount of biotinylated claudin-4 detected, together with a rapid increase of claudin-4 in the unbiotinylated fractions (supplementary material Fig. S1K), which further demonstrates that carbachol can induce claudin-4 internalization.

As shown in Fig. 2D, 10  $\mu\text{mol/l}$  cevimeline significantly decreased the amount of claudin-4 in a time-dependent manner, but did not affect the amount of occludin or E-cadherin. 4-DAMP pretreatment reversed the carbachol-induced claudin-4 decrease (Fig. 2E). Moreover, M3 knockdown by small interfering RNA (siRNA) completely abolished the carbachol-induced claudin-4 downregulation (Fig. 2E). We also detected the subcellular expression of M3 with or without M3 siRNA. In the untreated condition, M3 proteins were mainly located in the cytoplasm, with a small fraction (23.77%) at the cell membranes. After M3 knockdown, the total M3 amounts were decreased by  $51 \pm 4.8\%$  (mean  $\pm$  s.d.) compared with the group expressing scrambled siRNA,

but M3 expression at the cell membrane was greatly reduced to a very low level (8.75% of untreated total amounts). By contrast, carbachol still downregulated claudin-4, but not occludin or E-cadherin, in the cells pretreated with pirenzepine (supplementary material Fig. S1L,M). These results suggest that M3 plays a crucial role in regulating claudin-4 expression in SMG-C6 cells.

#### Carbachol alters the distribution of claudin-4 in the apical membrane

Immunofluorescence images showed that claudin-4 was continuously distributed in the cell membranes under untreated conditions (Fig. 3A). However, treatment with carbachol obviously diminished claudin-4 staining at some cell–cell contacts (white arrows), indicating that claudin-4 was partially removed from membranes. We further quantified the proportion of cells in which claudin-4 had been redistributed, and found that carbachol induced significant increases in claudin-4 ‘breaks’ from 10 to 60 min

(supplementary material Fig. S2A). The intensities of claudin-4-positive staining in both the membrane and overall were remarkably decreased by carbachol (supplementary material Fig. S2B,C). Furthermore, *x-z* plane images showed that the claudin-4-positive dots that were located in the apical region between two neighboring cells were dispersed by carbachol (Fig. 3A, lowest panel). Taken together, these observations indicate that carbachol decreases the amount of claudin-4 in the membrane.

To confirm whether this effect was specific, we also observed the distribution of other tight junction proteins. Occludin was continuously expressed in the membrane and its localization was unaffected by carbachol (Fig. 3B). Double staining against claudin-4 and occludin further showed that they colocalized in the cell–cell borders of untreated cells. Carbachol disrupted the continuity of claudin-4, but not occludin (white arrows in Fig. 3C, upper panels). Similar results were observed when ZO-1 was co-stained with claudin-4 (white arrows in Fig. 3C, lower panels). These results demonstrate that mAChR activation selectively alters claudin-4 distribution.

### Depletion or overexpression of claudin-4 alters the TER response upon treatment with carbachol

To elucidate the exact role of claudin-4 in mAChR-modulated paracellular permeability, we transfected claudin-4 small hairpin RNA (shRNA) into SMG-C6 cells and established stable knockdown cells. The mRNA and protein expression of claudin-4 was significantly reduced, while the expression of claudin-1, occludin, and ZO-1 were unaltered, except claudin-3 which showed an increase in both mRNA and protein levels (supplementary material Fig. S2D,E). The basal TER values of claudin-4-knockdown cells were slightly lower than scrambled cells, but the difference was not significant ( $530.3 \pm 73.39$  versus  $637.8 \pm 72.45$ , mean  $\pm$  s.d.). However, the carbachol-caused TER decreases were abolished in the claudin-4-knockdown cells (Fig. 4A), suggesting that claudin-4 plays a dominant role in mediating the carbachol-modulated TER decrease.

We further overexpressed claudin-4 by transfection with claudin-4 cDNA. Claudin-4 protein was significantly increased whereas occludin was unaffected (Fig. 4B). The basal TER values of the cells overexpressing claudin-4 showed a slight increase compared with the controls, but this was not significantly different ( $737.2 \pm 89.76$  versus  $639.1 \pm 82.14$ ). More importantly, in the cells overexpressing claudin-4, the carbachol-mediated decrease in the TER was partially reversed, and carbachol treatment significantly reduced the expression of claudin-4, but not occludin (Fig. 4C). These results again demonstrate that claudin-4 is the target selectively regulated by carbachol in SMG-C6 cells.

### Carbachol promotes claudin-4 phosphorylation in an ERK1/2-dependent manner

The possibility that tight junction function is regulated by post-transcriptional protein modification has been addressed in previous reports, especially the phosphorylation of tight junction proteins (González-Mariscal et al., 2008; Dörfel and Huber, 2012). To explore the molecular mechanism connecting mAChR to claudin-4, the serine- and threonine-phosphorylated proteins were extracted from SMG-C6 cells. The levels of bead-bound serine-phosphorylated claudin-4 compared with the amounts of claudin-4 in the input fractions (cell lysate) were significantly increased by carbachol. By contrast, neither occludin nor E-cadherin was phosphorylated at serine residues in carbachol-treated cells (Fig. 4D). However, the threonine-phosphorylated levels of these three components compared

with the corresponding inputs were not changed by carbachol (Fig. 4E). Moreover, the proteins immunoprecipitated with claudin-4 also confirmed that the serine-phosphorylated levels were higher in carbachol-treated cells, whereas the threonine-phosphorylated levels were unchanged (Fig. 4F).

Next, we examined the possible protein kinase that phosphorylated claudin-4. Extracellular signal-regulated kinase 1/2 (ERK1/2, also known as MAPK3 and MAPK1, respectively) is a classic serine/threonine kinase, and has been reported to modulate tight junction function and expression (Li and Mrsny, 2000; Samak et al., 2011). Carbachol treatments (0.01 to 10  $\mu$ mol/l) for 5 min induced more than twofold increases in the phosphorylated ERK1/2 (p-ERK1/2), and when incubated with 1  $\mu$ mol/l carbachol, the p-ERK1/2 levels were significantly elevated from 5 to 30 min. The total amounts of ERK1/2 did not change (Fig. 4G,H). Pretreatment with U0126 and PD98059 (5 and 20  $\mu$ mol/l, respectively), two ERK1/2 upstream kinase inhibitors, inhibited the carbachol-induced serine phosphorylation of claudin-4 (Fig. 4I). These results indicate that the carbachol-activated ERK1/2 specifically affects claudin-4 phosphorylation at serine residues.

### Claudin-4 phosphorylation is required for carbachol-modulated tight junction function

We then investigated the significance of ERK1/2-mediated claudin-4 phosphorylation in determining paracellular permeability. The carbachol-induced decreased claudin-4 was reversed by U0126 and PD98059 (Fig. 4J). Immunofluorescence images and quantification analysis revealed that the carbachol-induced claudin-4 discontinuities in the cell borders, and the decreased intensities in both membrane and overall cells, were blocked by U0126 or PD98059 (Fig. 4K; supplementary material Fig. S2F–H). Moreover, U0126 or PD98059 abolished the carbachol-induced TER decreases, as well as the increased flux for 4-kDa FITC-dextran (Fig. 4L,M). U0126 or PD98059 alone had no effect on these responses. These results suggest that ERK1/2-induced claudin-4 phosphorylation plays an important role in the carbachol-regulated content and distribution of claudin-4.

### S195 of claudin-4 is the specific site phosphorylated by carbachol

Claudin-4 has four membrane-spanning domains and the C-terminal residues can be phosphorylated by many cytoplasmic protein kinases (Lal-Nag and Morin, 2009). Four sites, S195, S199, S203 and S207 in rat and mouse claudin-4 (S194, S198, S202 and S206 of human, monkey and pig claudin-4) are highly conserved as shown in Fig. 5A, and these serine sites are specific in claudin-4 compared with other claudin family members, such as claudin-1 and claudin-3 (supplementary material Fig. S3A,B). To explore the specific site phosphorylated by carbachol, we constructed claudin-4 mutants, in which the serine (S) was replaced with alanine (A) (Fig. 5B). These base substitutions did not affect the synthesis of claudin-4 protein (Fig. 5C). Claudin-4 phosphorylation at serine residues was elevated in wild-type, S199A, S203A and S207A mutant cells after carbachol stimulation for 5 min, but the phenomenon was not seen in S195A mutant cells (Fig. 5D), indicating that S195 was the phosphorylated site for carbachol. Furthermore, in S195A mutant cells, both the downregulation of claudin-4 and the decreases in TER were attenuated, whereas these effects still existed in wild-type, S199A, S203A and S207A mutant cells (Fig. 5E–G). These findings demonstrate that carbachol modulates claudin-4 expression and tight junction function by triggering the phosphorylation of claudin-4 at S195.

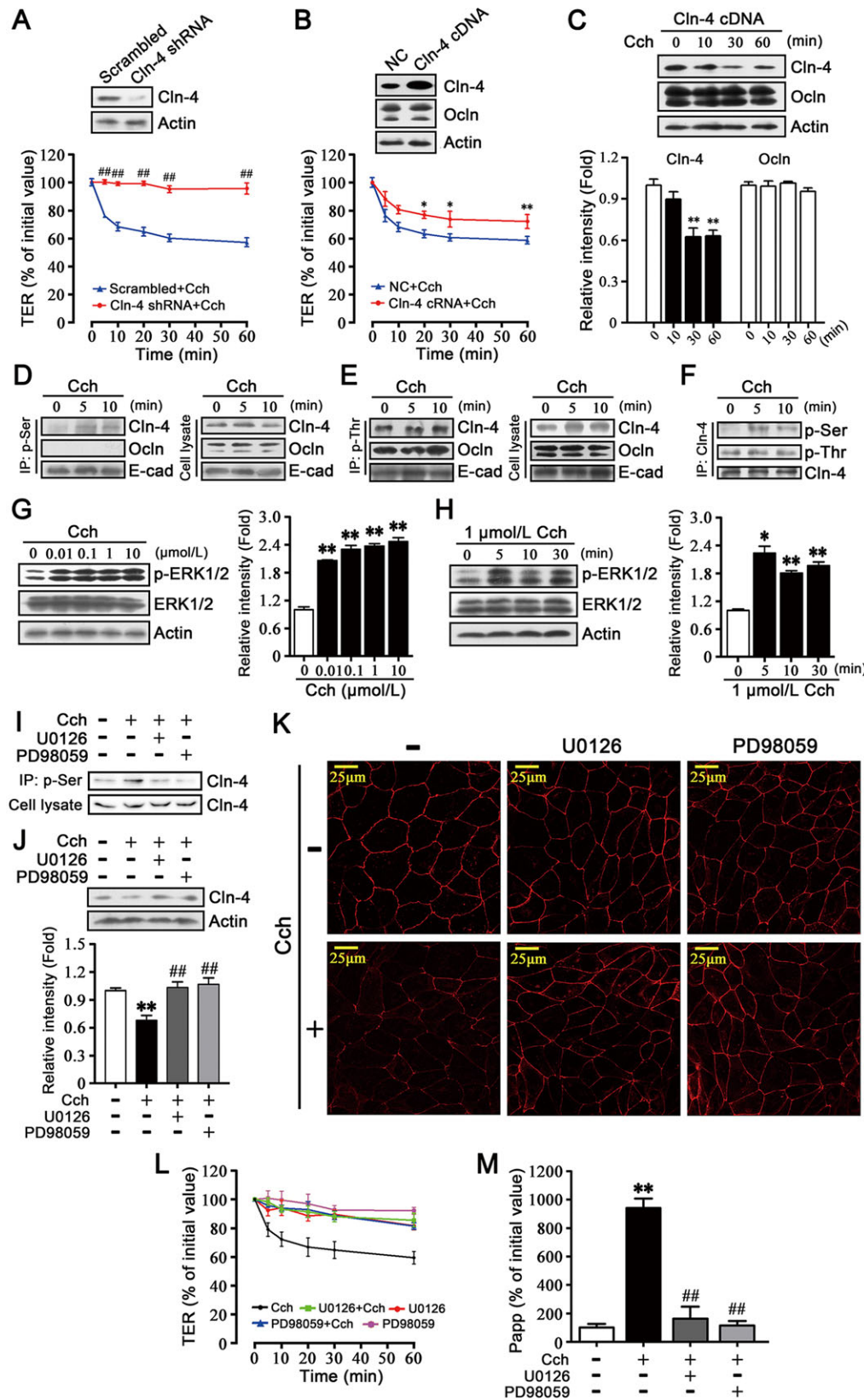


**Fig. 4. Claudin-4 is required to mediate the carbachol-induced increased paracellular permeability, and can be phosphorylated by ERK1/2.** (A) In the claudin-4-knockdown cells, the carbachol-induced TER decreases were significantly inhibited. (B) In the claudin-4-overexpressing cells, carbachol still caused TER decreases. NC, negative control. (C) Western blotting further revealed that carbachol decreased claudin-4 expression, but not occludin, in the claudin-4-overexpressing cells. \**P*<0.05 and \*\**P*<0.01 compared with the untreated cells. ###*P*<0.01 compared with scrambled shRNA controls. (D) The amount of serine-phosphorylated (p-Ser) claudin-4 (IP, immunoprecipitation) compared with the expression in the inputs (cell lysate) was increased by carbachol treatment for 5 and 10 min. By contrast, the ratios of occludin (Ocln) and E-cadherin (E-cad) phosphorylation were unaltered. (E) Among threonine-phosphorylated (p-Thr)-bound proteins, the amounts of claudin-4, occludin and E-cadherin were unaffected by carbachol. (F) Proteins immunoprecipitated with claudin-4 antibodies also identified that the levels of serine-phosphorylated, but not threonine-phosphorylated claudin-4, were obviously increased by carbachol. (G) Carbachol treatment for 5 min significantly increased the phosphorylation of ERK1/2 (p-ERK1/2). (H) 1 μmol/l carbachol elevated the levels of p-ERK1/2. (I) Pretreatment with ERK1/2 upstream inhibitors, U0126 and PD98059 (5 and 20 μmol/l, respectively), suppressed the carbachol-induced claudin-4 phosphorylation at serine residues. (J,K) Either U0126 or PD98059 abolished the carbachol-induced downregulation (J) and redistribution (K) of claudin-4. Each image is representative of three separate experiments performed in duplicate. (L,M) The carbachol-induced TER decreases (L) and increases in the apparent permeability coefficients (*P*<sub>app</sub>) for 4-kDa FITC-dextran (M) were abolished by either U0126 or PD98059 treatment. Values are mean±s.d. from three independent experiments performed in duplicate. \**P*<0.05 and \*\**P*<0.01 compared with the untreated cells. ###*P*<0.01 compared with the carbachol-treated cells.

**Carbachol promotes the interaction of claudin-4 and β-arrestin2**

To elucidate how carbachol modulated claudin-4, the expression of β-arrestin1 and β-arrestin2 were detected. The amounts of β-arrestin2 in the membrane fraction were increased within the first

10 min of carbachol treatment, but decreased at 30 and 60 min. However, the distribution of β-arrestin1 was unchanged (Fig. 6A). Coimmunoprecipitation showed that the level of β-arrestin2-bound claudin-4 was increased by carbachol, whereas no obvious bands of occludin were detectable, and the amounts of E-cadherin interacting

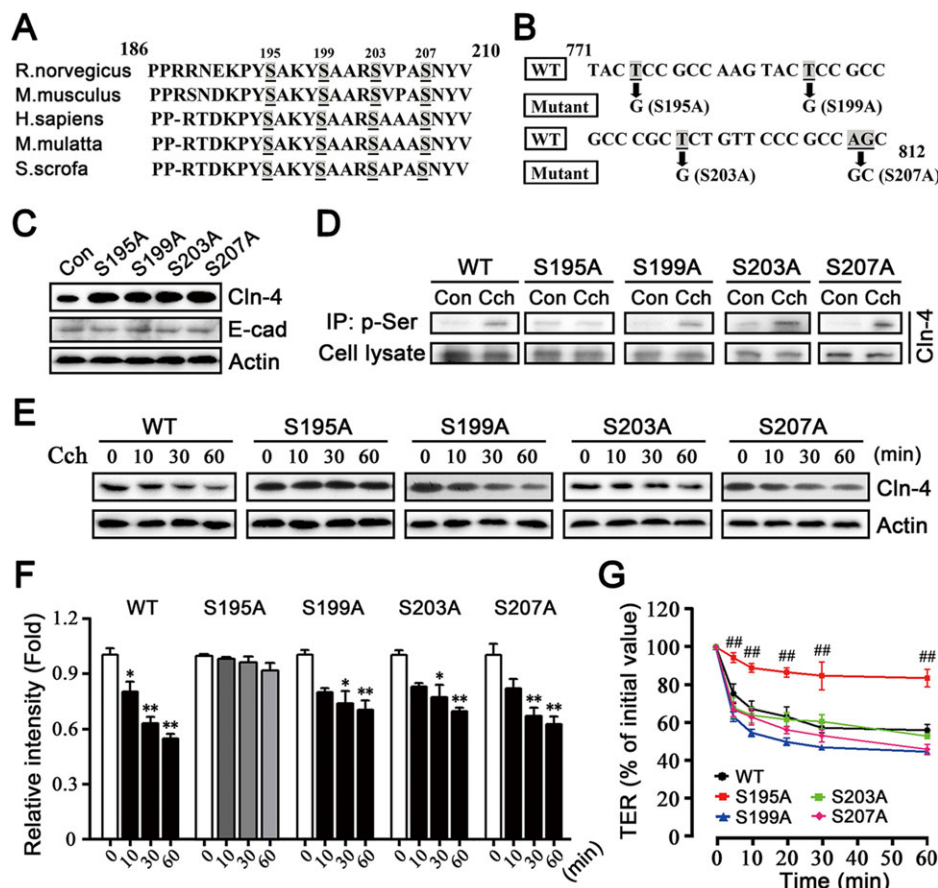


**Fig. 5. S195 of claudin-4 is the specific phosphorylated site for carbachol.**

(A) Multiple sequence alignments for the C-terminus cytoplasmic domain of claudin-4 from rat, mouse, human, monkey and pig. The potential conserved serine sites are marked in gray. (B) Four serine (S) sites, including S195, S199, S203 and S207 of rat claudin-4 were replaced with an alanine (A) residue. (C) Compared with the untreated cells (Con), claudin-4 expression was elevated in S195A, S199A, S203A and S207A cells. (D) In wild-type, S199A, S203A and S207A cells, carbachol increased the serine-phosphorylation of claudin-4; however, these effects were not detectable in S195A cells. Con, untreated cells. (E) The downregulation of claudin-4 disappeared in S195A cells, whereas it still observed in wild-type and other mutant cells. Statistical analysis of the western blot is shown in F. (G) S195A cells did not show a significant TER response to carbachol, whereas in wild-type and other mutant cells, carbachol still evoked TER decreases. Values are mean±s.d. from three independent experiments performed in duplicate. \* $P<0.05$  and \*\* $P<0.01$  compared with the untreated cells. ### $P<0.01$  compared with the wild-type cells.

with  $\beta$ -arrestin2 were not altered (Fig. 6B). By contrast, the levels of claudin-4, occludin and E-cadherin in  $\beta$ -arrestin1-bound proteins were unchanged (Fig. 6C). Furthermore, the proteins immunoprecipitated with claudin-4 revealed an increased  $\beta$ -arrestin2 amount in claudin-4-bound proteins upon treatment with carbachol within 10 min, which decreased at 30 and 60 min. For the analysis, we compared the ratio of the amount of  $\beta$ -arrestin2 in the bead-bound fraction to the amount of claudin-4 on the same membrane, which were  $1.39\pm 0.09$  ( $P<0.05$ ) and  $1.41\pm 0.08$  ( $P<0.05$ , mean±s.d.) after carbachol treatment for 5 and 10 min, respectively, returning to the untreated levels at 30 and 60 min ( $0.86\pm 0.03$  and  $1.03\pm 0.11$ , respectively). These results also confirm that there is a rapid interaction with  $\beta$ -arrestin2, but not  $\beta$ -arrestin1 (Fig. 6D), and indicate that mAChR activation promotes the interaction between claudin-4 and  $\beta$ -arrestin2.

#### Interaction between claudin-4 and $\beta$ -arrestin2 is required for the carbachol-modulated tight junction function

To address whether the interaction of claudin-4 with  $\beta$ -arrestin2 was involved in the carbachol-induced effects on claudin-4 and paracellular permeability, we designed specific siRNAs for knockdown of  $\beta$ -arrestin1 and  $\beta$ -arrestin2, respectively (Fig. 6E, supplementary material Fig. S4A).  $\beta$ -Arrestin1 knockdown did not affect the carbachol-induced claudin-4 decreases; however,  $\beta$ -arrestin2 knockdown significantly abolished this effect (Fig. 6F). In addition, the discontinuities and decreased intensity of claudin-4 in both apical membrane and overall cells caused by carbachol were also attenuated by  $\beta$ -arrestin2 knockdown, whereas  $\beta$ -arrestin1 knockdown did not influence these effects (Fig. 6G; supplementary material Fig. S4B–D). Furthermore, the carbachol-induced TER decreases were significantly blocked by knockdown of  $\beta$ -arrestin2, but not

$\beta$ -arrestin1 (Fig. 6H). The results suggest that  $\beta$ -arrestin2 is essential for mAChR to modulate claudin-4 content and distribution, as well as the paracellular permeability, and these effects might be due to the interaction between claudin-4 and  $\beta$ -arrestin2.

Next, we explored whether the association of claudin-4 with  $\beta$ -arrestin2 was triggered by claudin-4 phosphorylation. Either U0126 or PD98059 suppressed the carbachol-induced interaction between claudin-4 and  $\beta$ -arrestin2 (Fig. 6I, supplementary material Fig. S4E). However, in  $\beta$ -arrestin2 knockdown cells, carbachol still activated ERK1/2 (Fig. 6J). These results indicate that the ERK1/2-mediated claudin-4 phosphorylation is the upstream event prior to the interaction between claudin-4 and  $\beta$ -arrestin2. Moreover, in S195A mutant cells, the carbachol-induced claudin-4 and  $\beta$ -arrestin2 interaction was inhibited (Fig. 6K), which further suggests that phosphorylation of S195 is an essential prerequisite for the formation of the complex between claudin-4 and  $\beta$ -arrestin2.

#### Claudin-4 is internalized in a clathrin-dependent way

Previous studies have revealed that  $\beta$ -arrestin2 has a domain that directly interacts with clathrin, thereby evoking internalization or endocytosis of target membrane proteins through the clathrin-dependent pathway (Gavard and Gutkind, 2006; Min and Defea, 2011). Therefore, we examined whether an interaction between claudin-4 and clathrin was induced by carbachol. Results showed that their interaction was greatly enhanced by carbachol treatment for 5 min, and peaked at 10 min (Fig. 7A,B). To investigate the role of clathrin in determining claudin-4 properties, cells were preincubated with either 0.4 mol/l sucrose, an inhibitor of clathrin-dependent pathway, or transfected with clathrin siRNA. Results showed that the carbachol-induced claudin-4 decrease was blocked

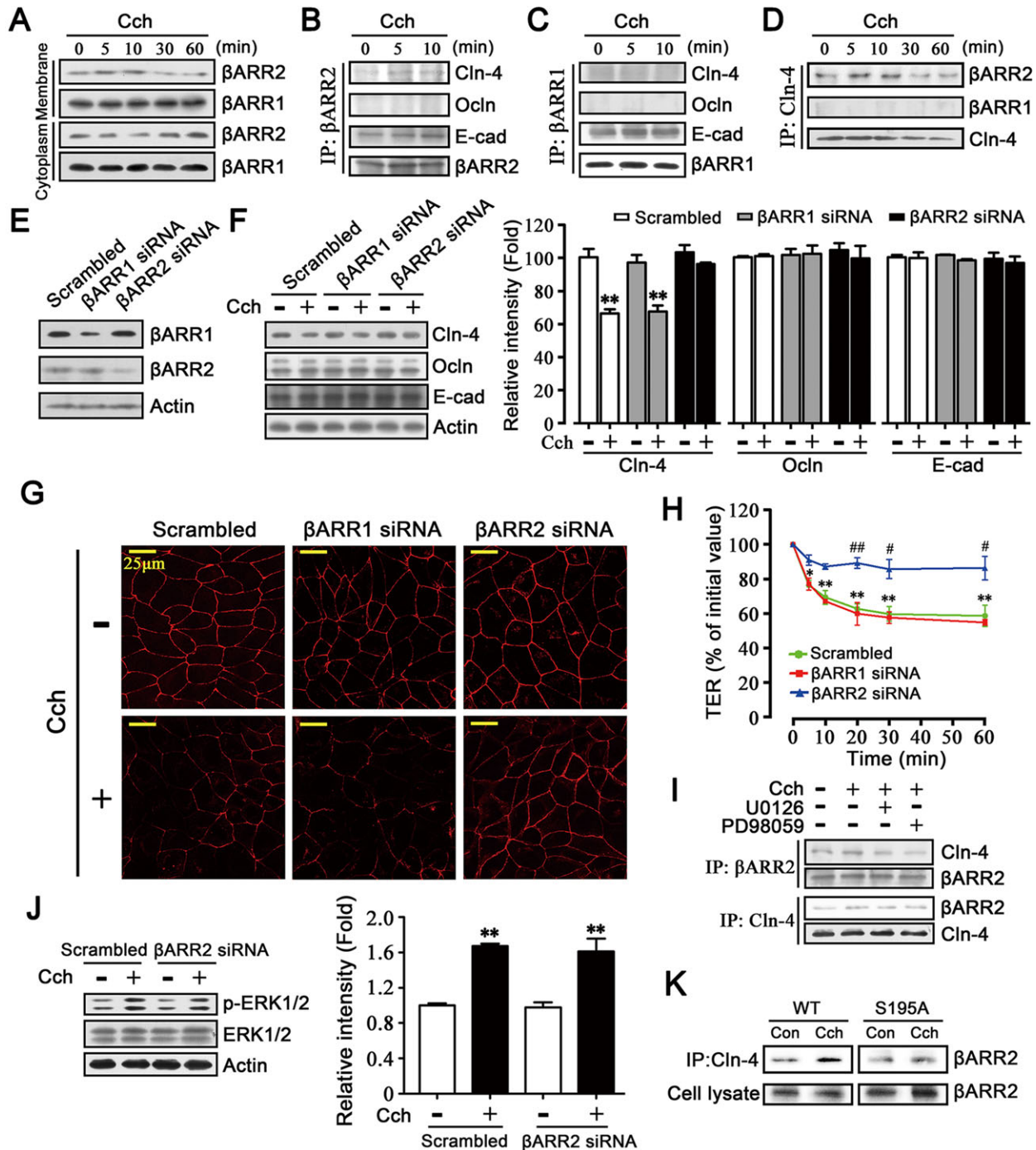


**Fig. 6. Interaction between claudin-4 and  $\beta$ -arrestin2 mediates the carbachol-induced alteration in claudin-4 properties and tight junction function.** (A) Carbachol (Cch) induced transient increases of  $\beta$ -arrestin2 ( $\beta$ ARR2) in the membrane fraction at 5 and 10 min, together with a decrease in the cytoplasm fraction. However, the  $\beta$ -arrestin1 ( $\beta$ ARR1) levels in these two fractions were unchanged. (B) Among the  $\beta$ -arrestin2-bound proteins (IP, immunoprecipitation), carbachol increased the amounts of claudin-4 (Cln-4), but no bands for occludin (Ocln) was present and there was no change for E-cadherin (E-cad). (C) Among the  $\beta$ -arrestin1-bound proteins, no obvious bands for claudin-4 or E-cadherin were detectable, and no change in E-cadherin was observed. (D) The proteins immunoprecipitated with claudin-4 antibodies also confirmed that carbachol caused an increased interaction between claudin-4 and  $\beta$ -arrestin2, but not  $\beta$ -arrestin1. (E) Western blot identification of transfection with  $\beta$ -arrestin1 and  $\beta$ -arrestin2 siRNAs, respectively. (F)  $\beta$ -Arrestin1 knockdown did not affect the carbachol-induced downregulation of claudin-4, whereas in  $\beta$ -arrestin2-knockdown cells, these effects were abolished. Statistical analysis of the western blot data is shown on the right. (G) Carbachol still induced claudin-4 redistribution in  $\beta$ -arrestin1-knockdown cells, whereas this effect was not seen in  $\beta$ -arrestin2-knockdown cells. Each image is representative of three separate experiments performed in duplicate. (H) Knockdown of  $\beta$ -arrestin1 did not affect the carbachol-induced TER decreases, whereas knockdown of  $\beta$ -arrestin2 abolished these effects. (I) Pretreatment with either U0126 or PD98059 blocked the carbachol-induced interaction between claudin-4 and  $\beta$ -arrestin2, as shown by the proteins immunoprecipitated with either  $\beta$ -arrestin2 (upper panels) or claudin-4 (lower panels). (J) In those  $\beta$ -arrestin2 knockdown cells, carbachol still enhanced the phosphorylation of ERK1/2. Statistical analysis of the western blot data is shown on the right. (K) In S195A mutant cells, the carbachol-induced increased interaction between claudin-4 and  $\beta$ -arrestin2 was blocked. WT, wild-type; Con, untreated cells. Values are mean  $\pm$  s.d. from three independent experiments performed in duplicate. \*\* $P$  < 0.01 compared with the untreated cells.

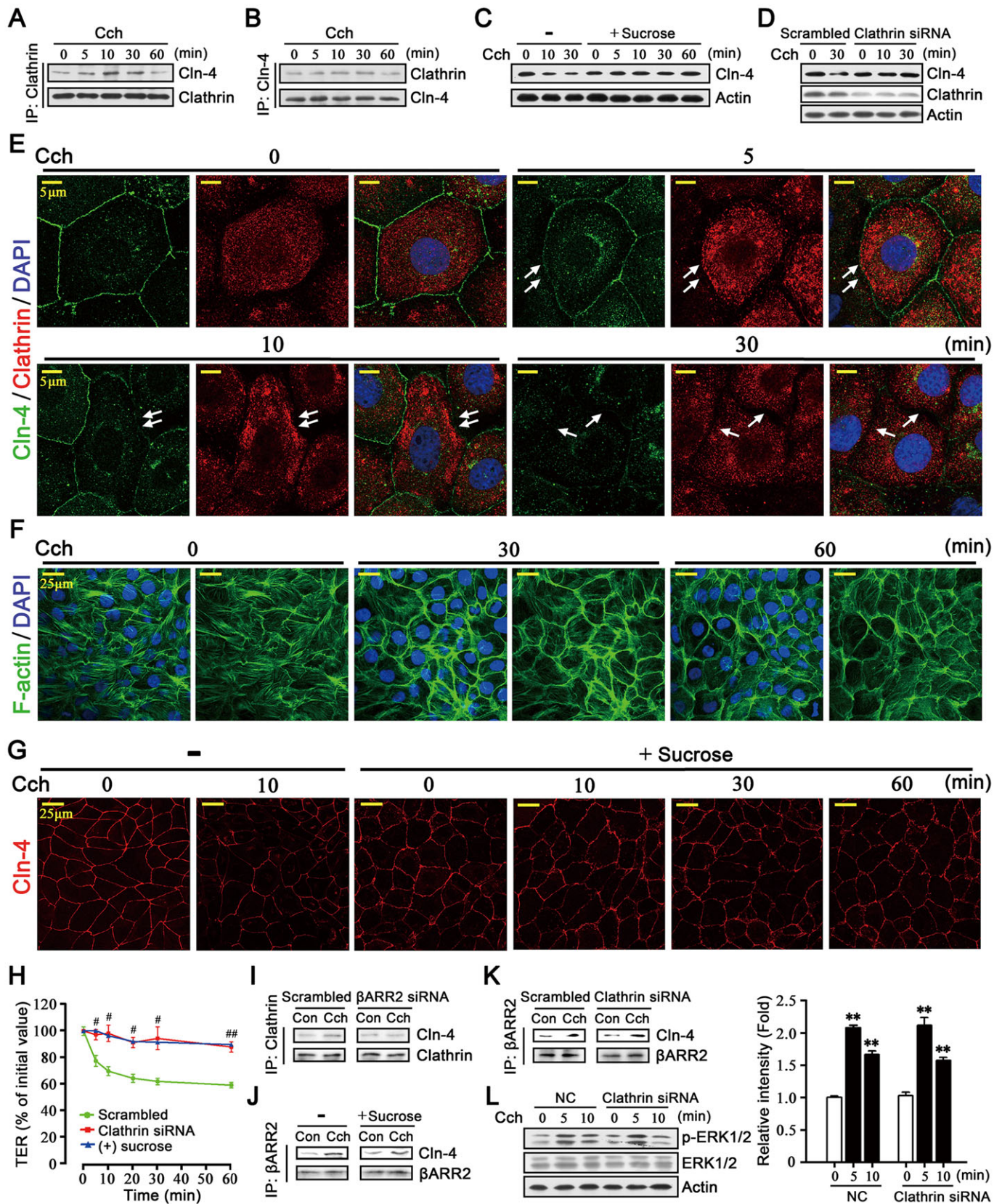


Fig. 7. See next page for legend.

by both sucrose and clathrin knockdown (Fig. 7C,D; supplementary material Fig. S4F,G). Pretreatment with dynasore (80 μmol/l), another clathrin-dependent endocytosis antagonist, showed similar

inhibitory effects on claudin-4 expression (supplementary material Fig. S4H). In addition, cell surface biotinylation analysis showed that the carbachol-induced claudin-4 decreases in the biotinylated

**Fig. 7. Claudin-4 is internalized via a clathrin-dependent pathway induced by carbachol.** (A) Among the clathrin-bound proteins, the amounts of claudin-4 (Cln-4) were increased by carbachol (Cch). (B) In the proteins immunoprecipitated (IP) with claudin-4 antibodies, the amounts of clathrin were also increased by carbachol. (C) Pretreatment with sucrose (0.4 mol/l), an inhibitor of clathrin-mediated internalization, blocked the carbachol-induced decreased claudin-4 expression. (D) Knockdown of clathrin by siRNA abolished the carbachol-induced claudin-4 downregulation. (E) Costaining images of claudin-4 (green) and clathrin (red) in SMG-C6 cells. Carbachol stimulation for 5 min caused an accumulation of clathrin from the cytoplasm towards the apical membrane (white arrows); at 10 min, the clathrin staining became reminiscent of vesicle-like clusters near the membranes; at 30 min, the distribution of clathrin was partially recovered whereas the apical claudin-4 staining was still diminished. Each image is a representative of three separate experiments performed in duplicate. (F) Carbachol induced the redistribution of F-actin (green) from the cytoplasm to the cell periphery at 30 min, and then recovered at 60 min. (G) The carbachol-induced claudin-4 redistribution was suppressed in the sucrose pretreated cells. (H) Both sucrose pretreatment and clathrin knockdown blocked the carbachol-induced TER decreases. (I) In  $\beta$ -arrestin2 knockdown cells, the carbachol-induced increased interaction between claudin-4 and clathrin was not detectable. (J,K) Carbachol enhanced the collaboration of claudin-4 and  $\beta$ -arrestin2 in either sucrose-pretreated (J) or clathrin-knockdown (K) cells. (L) Knockdown of clathrin did not affect the carbachol-activated ERK1/2 phosphorylation. A statistical analysis of the western blot data is shown on the right. \*\* $P < 0.01$  compared with the untreated cells. ## $P < 0.01$  and # $P < 0.05$  compared with the scrambled controls.

fraction and increases in the unbiotinylated fraction were abolished by dynasore (supplementary material Fig. S4I). These results indicate that clathrin is involved in carbachol-induced claudin-4 degradation and endocytosis.

To directly observe the involvement of clathrin, we performed immunofluorescence staining against clathrin. Images showed that carbachol treatment for 10 min caused obvious translocation of clathrin from the cytoplasm to cell membrane peripheries (white arrows in supplementary material Fig. S4J). Additionally, co-immunofluorescence staining showed that claudin-4 was mainly localized at the membranes when clathrin was dispersed in the cytoplasm under untreated conditions (Fig. 7E). After carbachol treatment for 5 min, clathrin-positive staining accumulated around cell membranes (white arrows); at 10 min, the staining of clathrin resembled vesicle-like clusters near the membrane where claudin-4 distribution began to be discontinuous; at 30 min, clathrin distribution was partially recovered. These images suggest that claudin-4 might be redistributed via clathrin-coated pits upon carbachol treatment.

To further confirm that clathrin-mediated internalization occurred, we stained cytoskeletal F-actin, which has been reported to participate in the formation of clathrin-coated vesicle (Merrifield et al., 2002; Smythe and Ayscough, 2006). Images showed that stress fibers, which are composed of F-actin, in the cytoplasm of untreated cells accumulated near the cell periphery after 30 min of carbachol treatment, and then partially recovered at 60 min (Fig. 7F), which is a similar dynamic pattern to that previously reported (Smythe and Ayscough, 2006). The results provide more evidence that mAChR activation evokes the clathrin-dependent internalization.

#### **Clathrin-dependent claudin-4 internalization is crucial to tight junction function and needs $\beta$ -arrestin2 recruitment**

As shown in Fig. 7G, sucrose pretreatment abolished the carbachol-induced claudin-4 redistribution. Quantification analysis showed that the increased claudin-4 breaks in the cell borders, as well as the decreased claudin-4 intensities at both the membrane and overall, were inhibited by sucrose (supplementary material Fig. S4K–M). Moreover, both sucrose and clathrin knockdown reversed the

carbachol-induced TER decreases (Fig. 7H). These results demonstrate that clathrin-dependent internalization plays an important role in determining claudin-4 properties and tight junction function.

We next explored the relationship between clathrin and  $\beta$ -arrestin2. In  $\beta$ -arrestin2 knockdown cells, the carbachol-induced interaction between claudin-4 and clathrin disappeared (Fig. 7I), whereas in cells either pretreated with sucrose or subjected to clathrin knockdown, carbachol still enhanced the interaction between claudin-4 and  $\beta$ -arrestin2 (Fig. 7J,K). These data suggest that clathrin is the downstream molecule recruited by  $\beta$ -arrestin2. Additionally, clathrin knockdown did not affect the carbachol-activated ERK1/2 phosphorylation, whereas dynasore preincubation did not influence the carbachol-induced phosphorylation of claudin-4 at serine residues (Fig. 7L; supplementary material Fig. S4N). Moreover, in S195A mutant cells, the carbachol-induced increased interaction between claudin-4 and clathrin was blocked (supplementary material Fig. S4O). Taken together, these results indicate that claudin-4 phosphorylation is required for its endocytosis through the clathrin-dependent pathway.

#### **Carbachol downregulates claudin-4 protein through ubiquitylation**

Previous studies have reported that the internalized proteins can be either recycled to the membrane or degraded in the cytoplasm through the ubiquitin–proteasome pathway (Gavard and Gutkind, 2006; Yeh et al., 2011). Accordingly, we decided to determine whether the carbachol-induced intracellular claudin-4 was degraded by ubiquitylation. There was little claudin-4 ubiquitylation in the basal condition, but carbachol increased claudin-4 ubiquitylation at ~22 kDa as well as polyubiquitylation in a time-dependent manner (Fig. 8A). Moreover, carbachol increased the interaction between ubiquitin and claudin-4, as shown by elevated amounts of claudin-4 in the ubiquitin-bound proteins compared with that in the input controls (Fig. 8B), suggesting that claudin-4 is specifically ubiquitylated in response to carbachol treatment. Preincubation with MG132 (10  $\mu$ mol/l), an ubiquitin–proteasome pathway inhibitor, blocked the carbachol-induced claudin-4 decreases (Fig. 8C). Additionally, MG132 partially and significantly reversed the carbachol-induced TER decreases (Fig. 8D). These data suggest that carbachol-induced claudin-4 ubiquitylation contributes, at least in part, to the downregulation of claudin-4 which in turn leads to the increase in paracellular permeability.

Furthermore, we detected the distribution of claudin-4 after treatment with MG132. Although MG132 blocked the carbachol-induced decrease in claudin-4 fluorescence intensities, the plasma membrane staining showed indents with punctate protrusions surrounded by positive dots after treatment with carbachol for 30 and 60 min (white arrows in Fig. 8E), which is a similar phenomenon to that observed in the clathrin-dependent endocytosis process. The images reveal that MG132 abolishes the carbachol-induced claudin-4 degradation in the cytoplasm, but does not affect claudin-4 endocytosis and removal from the cell membranes.

We also assessed the amount of ubiquitylated claudin-4 in the cells expressing the mutated claudin-4 S195A. Unlike in wild-type cells, the carbachol-induced increase in ubiquitylated claudin-4 was not seen in S195A mutant cells (Fig. 8F), which indicates that the phosphorylation of claudin-4 is a prerequisite for its ubiquitylation.

#### **DISCUSSION**

There are three major findings presented by our study. First, we demonstrate that claudin-4 is the specific target that mediates the

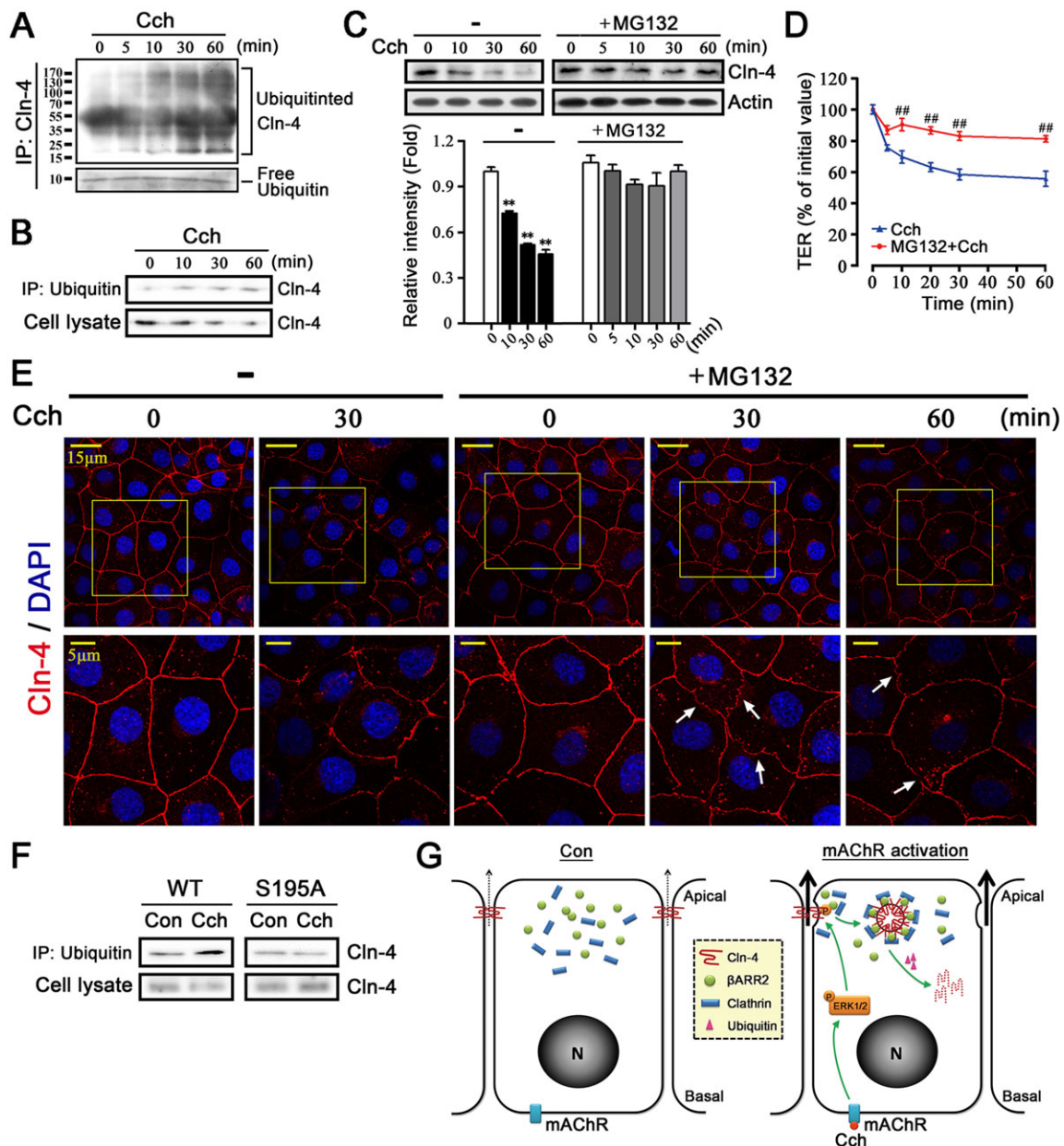


**Fig. 8. Carbachol induces claudin-4 degradation through a ubiquitin-dependent pathway.** (A) A co-immunoprecipitation (IP) assay showed that the ubiquitylated claudin-4 (Cln-4) was obviously increased after carbachol (Cch) treatment for 10, 30 and 60 min. (B) An ubiquitin immunoprecipitation showed that the amounts of claudin-4 compared with the inputs were elevated by carbachol. (C) Pretreatment with MG132 (10  $\mu\text{M}$ ), an inhibitor of the ubiquitin–proteasome pathway, blocked the carbachol-induced claudin-4 degradation. (D) MG132 significantly inhibited the TER responses to carbachol. Values are mean  $\pm$  s.d. from three independent experiments performed in duplicate.  $**P < 0.01$  compared with the untreated cells.  $###P < 0.01$  compared with the solvent controls. (E) The carbachol-induced claudin-4 fluorescent intensity decreases were blocked by MG132, and the plasma membrane staining show indents with punctate protrusions surrounded by positive dots (white arrows). Each image is a representative of three separate experiments in duplicate. (F) In S195A mutant cells, the carbachol-induced enhanced ubiquitylated claudin-4 was not seen. (G) Schematic illustrations showing the mechanism of mAChR-modulated increased paracellular permeability.

mAChR-modulated paracellular permeability in submandibular epithelial cells. Activation of mAChR, predominately through M3, increases paracellular permeability by inducing downregulation and redistribution of claudin-4. Second, an ERK1/2-dependent claudin-4 phosphorylation at S195, but not S199, S203 or S207, is essential for mAChR to modulate claudin-4 properties and tight junction function. Third, the phosphorylated claudin-4 recruits  $\beta$ -arrestin2, which serves as an adaptor protein to interact with clathrin, resulting in the clathrin-dependent claudin-4 internalization. The internalized claudin-4 is further partially degraded by ubiquitylation.

These results suggest that ERK1/2,  $\beta$ -arrestins, clathrin and the ubiquitin signaling pathway are involved in the mAChR-modulated paracellular transport in epithelial cells.

The cholinergic system plays an important role in fluid and electrolyte transport in epithelia. For example, mAChR agonists and antagonists are commonly used to treat impaired saliva and tear secretion (Melvin et al., 2005; Morimoto-Tochigi et al., 2010). However, it is noteworthy that material transport across epithelial cells can be accomplished by either transcellular or paracellular pathways (Tsukita et al., 2001). The effect of mAChR activation on

transcellular pathway has already been well investigated, including the opening of ion channels and the trafficking of water transporters like aquaporin5 in salivary glands (Ishikawa et al., 1998; Melvin et al., 2005). However, studies on the relationship between mAChR and paracellular transport are still limited. MDCK cells develop a TER when they are switched from a low  $\text{Ca}^{2+}$  to a normal  $\text{Ca}^{2+}$  medium; however, carbachol inhibits this development of TER (Balda et al., 1991). In the isolated rat submandibular gland perfusion model, both carbachol and pilocarpine significantly increase the transport of fluorescently labeled tracers (e.g. Lucifer Yellow) from basolateral spaces of acini into intercellular canaliculi; in rapidly frozen specimens, tight junction strands as well as actin filament network, are rearranged roughly and become interrupted after carbachol stimulation (Segawa, 1994; Hashimoto et al., 2003; Hashimoto and Murakami, 2009). These data suggest that epithelial tight-junction-based paracellular transport is also controlled by the cholinergic system. Here, we found that in salivary epithelial SMG-C6 cells, both the mAChR nonselective agonist carbachol and the M3-specific agonist cevimeline significantly decreased TER values and increased paracellular permeability for small macromolecules, and that pretreatment with the M3-specific antagonist 4-DAMP, but not the M1-specific antagonist pirenzepine, abolished these effects. The results provide new evidence that activation of mAChR, predominately through M3, directly increases the paracellular permeability of epithelial cells.

The well-balanced amounts of tight junction proteins in the apical cell membranes guarantee their function as regulators for paracellular transport (Schulzke et al., 2012). Previous studies have shown that the impact on paracellular permeability induced by different stimulators can be either reversible or irreversible due to their effects on the content and distribution of tight junctions (Murakami et al., 2009; Yeh et al., 2011). Here, we found that carbachol removal caused a partial TER recovery at 5 min, but was followed by irreversible TER responses at both 10 and 30 min, which implies that mAChR activation modulates paracellular permeability by influencing the content and distribution of tight junctions. Thus, we investigated which specific tight junction component was involved in the mAChR-modulated paracellular permeability. Carbachol or cevimeline significantly reduced the amounts of claudin-4, but not other tight junction or adherens junction components, and this downregulation could be blocked by either 4-DAMP or M3 knockdown, but not by pirenzepine, indicating that claudin-4 is the specific target for mAChR, and its expression is downregulated mainly through M3 in SMG-C6 cells.

It has been shown in previous electron micrograph studies that, upon treatment with stimuli, tight junctions can localize in the cytosolic vesicles, suggesting that the internalization or endocytosis of tight junctions is a common mechanism by which the epithelial paracellular permeability is altered (Staehelin, 1973; Madara, 1990; Matsuda et al., 2004). Recently, by using immunofluorescence staining and transfection of fluorescently tagged tight junction proteins, the specific tight junction component involved in the internalization has been further determined. For example, occludin internalization occurs upon exposure to cytokines, bacteria, toxins and  $\text{Ca}^{2+}$  depletion (Simonovic et al., 2000; Hopkins et al., 2003; Sheth et al., 2003; Muza-Moons et al., 2004; Shifflett et al., 2005; Wang et al., 2005). Claudin-3 internalization is seen during the intracellular movement of epithelial monolayers in Eph4 cells (Matsuda et al., 2004). Here, by using membrane and cytoplasm fraction extraction and a cell surface biotinylation assay, we found that carbachol induced constant decreases in the amount of claudin-4 in the membrane fraction, together with a rapid increase in the

amount in the cytoplasm fraction, indicating that carbachol causes a prompt intracellular trafficking of claudin-4 followed by degradation. Immunofluorescence staining further showed that the apical continuities of claudin-4 were disturbed by carbachol, whereas occludin and ZO-1 were unaffected. Moreover, statistical analysis revealed that the intensities of both membrane and overall staining were remarkably diminished. These results suggest that mAChR activation also modulates claudin-4 distribution as well as its content in epithelial cells.

Claudins are crucial structural and functional transmembrane components of tight junctions. The extracellular loops of claudins interact with each other to seal the cellular sheet and regulate paracellular transport between luminal and basolateral spaces (Lal-Nag and Morin, 2009). Claudin-4 has been detected in diverse epithelia, such as salivary, renal, lung, intestinal and epidermal cells (Akazawa et al., 2013; Cong et al., 2013; Gong et al., 2014; Kage et al., 2014; Shrestha et al., 2014). In rat submandibular SMIE cells, overexpression of claudin-4 increases TER and decreases the epithelial permeability of 70 kDa dextran (Michikawa et al., 2008). Alterations in claudin-4 expression and localization are shown in the labial salivary glands from Sjögren's syndrome patients (Ewert et al., 2010). In MDCK cells, overexpression of claudin-4 decreases transepithelial conductance by decreasing the paracellular permeability for  $\text{Na}^+$  (Van Itallie et al., 2001). In cultured pig kidney epithelial cells, claudin-4 knockdown decreases  $\text{Cl}^-$  permeability through the paracellular pathway (Hou et al., 2006). These studies suggest that claudin-4 might be necessary and responsible for epithelial paracellular transport. Here, we found that knockdown or overexpression of claudin-4 slightly affected the TER baseline of SMG-C6 cells. In the claudin-4 stable knockdown cells, the expression of claudin-3 was increased, whereas that of other tight junction components was unaffected. Given that claudin-4 has the most similarity to claudin-3 in structure compared with other claudins, we speculate that the upregulation of claudin-3 might be a partial compensation for claudin-4, and as a result, claudin-4 stable knockdown cells show only a slight, but not significant decrease in the TER. However, the carbachol-induced TER decreases were completely abolished in claudin-4-deficient cells. In addition, carbachol still reduced TER values and claudin-4 protein levels in claudin-4-overexpressing cells. These results indicate that claudin-4 is required to mediate the carbachol-induced increase in paracellular permeability in epithelial cells.

We next explored the signaling pathway linking mAChR to claudin-4. The relationship between tight junction phosphorylation and tight junction function was first reported in the late 1980s, showing that ZO-1 is more phosphorylated in low-resistance MDCK cells than in high-resistance monolayers (Stevenson et al., 1989). Since then, increasing numbers of studies have revealed that tight junction proteins are regulated by phosphorylation.  $\text{H}_2\text{O}_2$  induces increased threonine phosphorylation of occludin in Caco-2 cells, together with a redistribution of occludin and ZO-1 from tight junctions into the cytoplasm and an increased paracellular permeability (Basuroy et al., 2006). Vascular endothelial growth factor (VEGF)-induced occludin phosphorylation contributes to occludin trafficking from the cell border to the cytoplasm endosome with subsequent ubiquitylation and increased vascular permeability (Murakami et al., 2009). Inhibition of MEK1 attenuates ZO-1 phosphorylation and enhances tight junction assembly (Chen et al., 2000). These data suggest that tight junction phosphorylation might play a crucial role in determining tight junction content, distribution and function. Here, we found that carbachol selectively enhanced claudin-4 phosphorylation at serine residues, but not

threonine residues, and this effect was abolished by two ERK1/2 inhibitors, suggesting that the mAChR-induced claudin-4 phosphorylation is accomplished through ERK1/2. Furthermore, when claudin-4 phosphorylation was blocked by ERK1/2 inhibitors, the carbachol-induced downregulation and redistribution of claudin-4, as well as TER decreases, were significantly inhibited, which indicates that the ERK1/2-dependent claudin-4 phosphorylation is responsible for the mAChR-modulated paracellular permeability.

Nowadays, the analysis by point mutation of particular phosphorylated residues in tight junction proteins contributes to a better understanding of the significance of tight junction phosphorylation. For example, claudin-3 phosphorylation at T192, which is mediated by PKA, disturbs the barrier function of tight junctions (D'Souza et al., 2005); phosphorylation of T770 or T772 of ZO-1 leads to its disassembly from tight junctions and affects the endothelial barrier permeability (Chattopadhyay et al., 2014). However, to date, there are limited studies referring to the phosphorylation sites of claudin-4. The phosphorylation of human claudin-4 at S194 and T189, which is mediated by PKC $\epsilon$  disrupts tight junction barrier function in ovarian cancer cells (D'Souza et al., 2007). Another study have shown that atypical-PKC-induced phosphorylation of claudin-4 S194 phosphorylation is required for tight junction formation in a human keratinocyte cell line (Aono and Hirai, 2008). These studies indicate that tight junction proteins can be phosphorylated at particular sites. However, it is notable that even the same site might trigger different effects given that the phosphorylation can be achieved by different kinases upon different cell types. Here, by constructing four conserved serine mutants, we found that S195, but not S199, S203 or S207 of rat claudin-4, was the specific site phosphorylated upon carbachol treatment. Moreover, in S195 mutant cells, the carbachol-induced claudin-4 downregulation and TER decreases were abolished, which suggests that phosphorylation of claudin-4 at S195 is essential for mAChR to modulate claudin-4 content and tight junction function in SMG-C6 cells.

$\beta$ -Arrestins were originally discovered to desensitize GPCRs by binding to the serine or threonine residues the became phosphorylated upon agonist treatment, thereby inducing their internalization (Lohse et al., 1990; Krupnick and Benovic, 1998). Recently,  $\beta$ -arrestin1 and  $\beta$ -arrestin2 have been found to mediate internalization of proteins that are not GPCRs, such as transient receptor potential vanilloid subtype 4 and vascular endothelial cadherin (Shukla et al., 2010; Yeh et al., 2011). Here, we revealed that mAChR activation promoted the interaction between claudin-4 and  $\beta$ -arrestin2, but not  $\beta$ -arrestin1. Knockdown of  $\beta$ -arrestin2 abolished the carbachol-induced downregulation and redistribution of claudin-4, as well as the TER decreases. These data indicate that  $\beta$ -arrestin2 is required for the regulation of claudin-4. Furthermore, we found that inhibition of claudin-4 phosphorylation by ERK1/2 inhibitors abolished the interaction between claudin-4 and  $\beta$ -arrestin2, whereas knockdown of  $\beta$ -arrestin2 did not affect the carbachol-induced ERK1/2 phosphorylation. In addition, the formation of the claudin-4 and  $\beta$ -arrestin2 complex induced by carbachol was inhibited in S195A mutant cells. These results indicate that  $\beta$ -arrestin2 is recruited by claudin-4 phosphorylation at S195 that is mediated by ERK1/2, and thereby promoting the carbachol-induced downregulation and redistribution of claudin-4.

Internalization or endocytosis is the process through which the plasma membrane invaginates into the cytosol, leading to the production of vesicles comprising the target membrane proteins (Kumari et al., 2010). Internalization by clathrin-coated vesicles has been visualized by electron microscopy for over 40 years (Roth and

Porter, 1964). In the process of internalization, clathrin is first recruited to assemble at the cell membrane, then forms clathrin-coated pits to move the target proteins into the cells, and finally the pits lose their coats and deliver the endocytic vesicles to the early endosome (Smythe and Ayscough, 2006). Previous studies have revealed that  $\beta$ -arrestin1 and  $\beta$ -arrestin2 have a domain that directly interacts with clathrin, and thereby triggering the endocytic events via clathrin-coated pits (Gavard and Gutkind, 2006; Min and Defea, 2011). It is noteworthy that tight junction proteins, including claudin-1, claudin-4, occludin and ZO-1, are internalized by clathrin in T84 epithelial cells (Ivanov et al., 2004). Here, we found that carbachol enhanced the interaction between claudin-4 and clathrin, and led to the formation of vesicle-like clusters of clathrin, indicating that claudin-4 might be internalized within clathrin-coated pits. In addition, F-actin was also dynamically rearranged to accumulate around cell membranes, a similar pattern to assist the remodeling of cell surface to allow intracellular movement of vesicles in previous reports (Smythe and Ayscough, 2006). Moreover, inhibition of clathrin pathway by either pretreatment with sucrose and dynasore or clathrin knockdown abolished the downregulation and redistribution of claudin-4, as well as the TER decreases, induced by carbachol. By using inhibitors and siRNAs,  $\beta$ -arrestin2 was further identified to serve as an adaptor protein between claudin-4 and clathrin. Furthermore, formation of the carbachol-induced claudin-4 and clathrin complex was abolished in S195A mutant cells. These results indicate that clathrin participates in the mAChR-modulated claudin-4 internalization through  $\beta$ -arrestin2 recruitment, and claudin-4 phosphorylation at S195 is a prerequisite for claudin-4 endocytosis.

Moreover, the event following claudin-4 internalization remained unclear. Previous studies have reported that the internalized proteins can be either recycled or degraded through the rapid ubiquitin–proteasome pathway, resulting in the reversible or irreversible effect on tight junction content and function (Gavard and Gutkind, 2006; Murakami et al., 2009; Yeh et al., 2011). Based on the above results, we suspected that claudin-4 might be degraded following its internalization. The results showed that the amount of the specifically ubiquitylated claudin-4 was greatly enhanced by carbachol, and MG132 treatment abolished the carbachol-induced claudin-4 downregulation and TER decreases. Immunofluorescence images further revealed that MG132 abolished the carbachol-induced claudin-4 degradation, but did not affect claudin-4 endocytosis. Additionally, carbachol did not cause claudin-4 ubiquitylation in S195A mutant cells. These data suggest that intracellular claudin-4 ubiquitylation is involved in the carbachol-induced claudin-4 downregulation and the increase in paracellular permeability, and claudin-4 phosphorylation at S195 is an essential event for its ubiquitylation, which is probably mediated by recruitment of  $\beta$ -arrestin2 and clathrin.

In conclusion, we provide the first evidence that activation of mAChR induces phosphorylation of claudin-4 in an ERK1/2-dependent manner, and downregulation of claudin-4 through  $\beta$ -arrestin2-, clathrin- and ubiquitin-dependent signaling pathway. These effects on the content and distribution of claudin-4 are necessary for and contribute to the eventual increased paracellular permeability of SMG-C6 cells (a schematic illustration is shown in Fig. 8G). Taken together, these findings demonstrate a crucial role for claudin-4 in the mAChR-modulated paracellular permeability of epithelial cells, and enrich our understanding of the mechanism involved in the mAChR-mediated modulation of tight junction properties.

## MATERIALS AND METHODS

### Cell culture

The rat epithelial SMG-C6 cells were cultured at 37°C in a humidified 5% CO<sub>2</sub> atmosphere in DMEM/F12 (1:1 mixture) medium containing 2.5% fetal bovine serum, 5 µg/ml transferrin, 1.1 µmol/l hydrocortisone, 0.1 µmol/l retinoic acid, 2 nmol/l thyronine T<sub>3</sub>, 5 µg/ml insulin, 80 ng/ml epidermal growth factor, 50 µg/ml gentamicin sulfate, 5 mmol/l glutamine, 100 U/ml penicillin, and 100 µg/ml streptomycin. All the constituents were purchased from Sigma-Aldrich (Sigma-Aldrich, MO).

### Reagents and antibodies

Carbachol, 4 kDa and 40 kDa FITC–dextran, cevimeline, 4-DAMP, DMSO, pirenzepine, FITC-labeled phalloidin, PD98059, U0126, sucrose, dynasore and MG132 were purchased from Sigma-Aldrich (Sigma-Aldrich, MO). Antibodies against claudin-1 (BS6778, 1:500), claudin-4 (BS1068, 1:500), E-cadherin (BS1098, 1:500), β-arrestin1 (BS2213, 1:500) and ubiquitin (BS1487, 1:500) were from Bioworld Technology (Minneapolis, MN). Antibodies against occludin (331500, 1:500), claudin-3 (341700, 1:500), ZO-1 (402200, 1:500), and Alexa-Fluor®-594-conjugated claudin-4 (329494, 1:500) were from Life Technologies (Carlsbad, CA). Antibodies to ERK1/2 (sc-93, 1:500), p-ERK1/2 (sc-7383, 1:500), p-Ser (sc-81515, 1:200), p-Thr (sc-5267, 1:200), β-arrestin2 (sc-13140, 1:500), clathrin (sc-12735, 1:500) and actin (sc-1616, 1:1000) were from Santa Cruz Biotechnology (Santa Cruz, CA).

### TER measurement and paracellular tracer flux assay

Confluent monolayers of SMG-C6 cells were grown in 24-well Corning Transwell™ chambers (polycarbonate membrane, filter pore size 0.4 µm, area 0.33 cm<sup>2</sup>; Costar) for 7 days and then TER was measured at 37°C using an Epithelial Volt Ohm Meter (EVOM; WPI, FL). TER values were calculated by subtracting the blank filter (90 Ω) and by multiplying the surface area of the filter. All measurements were performed on a minimum of triplicate wells.

For paracellular tracer flux assay, 1 mg/ml 4 kDa or 40 kDa FITC–dextran was added to the medium in the apical sides and the samples were collected from the basal sides after incubation for 3 h. Using a fluorometer (BioTek, VT), the apparent permeability coefficient ( $P_{app}$ ) was determined as the increase in the amount of tracer per time per filter area.

### Western blotting

The cells were homogenized in lysis buffer (containing 50 mmol/l Tris-HCl, 150 mmol/l NaCl, 1 mmol/l EDTA, 1 mmol/l phenylmethylsulfonyl fluoride, 1% Triton X-100, 0.1% SDS, and 0.1% sodium deoxycholate, pH 7.2) and centrifuged at 1000 *g* for 10 min at 4°C. The supernatant were collected and protein concentration was determined by the Bradford method. Equal amounts of proteins (40 µg) were separated on a 9% SDS-PAGE gel and transferred onto a polyvinylidene difluoride membrane. The membranes were blocked with 5% non-fat milk, probed with primary antibodies at 4°C overnight, and then incubated with horseradish peroxidase (HRP)-conjugated secondary antibodies. Immunoreactive bands were visualized with enhanced chemiluminescence (Thermo Scientific Pierce, USA). The densities of bands were quantified with the Image J Software (National Institutes of Health, MD).

### Reverse transcription PCR and real-time PCR

Total RNA extraction and reverse transcription were performed as previously reported (Cong et al., 2013). The primer sequences for rat tight junction components are shown in supplementary material Table S1. For real-time PCR, DyNAmo™ ColorFlash SYBR Green qPCR Kit (Thermo Fisher Scientific) were used on a PikoReal Real-Time PCR System (Thermo Fisher Scientific) and analyzed using PikoReal 2.0 software.

### Preparation of membrane and cytoplasm fractions

Membrane and cytoplasm protein fractions were separated by Nucl-Cyto-Mem Preparation Kit (Appligen Technologies Inc., Beijing, China) according to the manufacturer's protocol.

### Cell surface biotinylation assay

Cell surface proteins were biotinylated by using a Pierce Cell Surface Protein Isolation Kit (Thermo Scientific, Rockford, IL) according to the manufacturer's protocol. Proteins from the biotinylated and unbiotinylated (the flow-through unbound proteins) fractions were analyzed by western blotting.

### Immunofluorescence staining

Immunofluorescence staining was performed as previously reported (Cong et al., 2013). Fluorescence images were captured on a confocal microscope (Leica TCS SP5, Wetzlar, Germany). The percentage of redistributed claudin-4 was represented by the proportion of cells in which claudin-4 breaks in staining greater than 4 µm were visible in lower magnification images of at least 100 cells. For quantification analysis, the fluorescent intensities of claudin-4 in ten random cells from each group were averaged, and data were reported as the relative intensity of claudin-4 in cell membrane and the relative overall intensity of claudin-4.

### Knockdown of M3 receptor, β-arrestin1, β-arrestin2 and clathrin

The SMG-C6 cells were cultured to 80% confluence and then transfected with siRNA of interests by using MegeTran 1.0 (Origene Technologies, MD, USA) according to the manufacturer's instructions. To suppress the expression levels, the siRNAs and non-specific negative control were purchased from Sigma-Aldrich: M3 receptor (SASI\_Rn01\_00041487), β-arrestin1 (SASI\_Rn01\_00105287), β-arrestin2 (SASI\_Rn01\_00090533) and clathrin (SASI\_Rn01\_00041427).

### Stable cell line generation

For knockdown of claudin-4, shRNA constructs and scrambled control were purchased from Origene Technologies (TG701533; MD, USA) and transfected by using MegeTran 1.0. Selection was achieved with 4 µg/ml puromycin, which was added into the medium after transfection for 2 weeks. Resistant cells were sorted to obtain only GFP-expressing cells under a fluorescence microscope. Cells were maintained in medium that was supplemented with 1 µg/ml puromycin, and then harvested for the following studies.

For overexpression of claudin-4, a cDNA clone was purchased from Origene Technologies (RR210685; MD, USA). The plasmid was transfected into the cells by MegeTran 1.0. The cells were subjected to G418 selection (1 mg/ml), and the independent clones were isolated and passaged. After 2 weeks, the cells were maintained in the medium containing 0.5 mg/ml G418.

### Claudin-4 mutant construction

S195, S199, S203 and S207 of rat claudin-4 were replaced with alanine using the Fast Mutagenesis System (Beijing TransGen Biotech Co. Ltd., Beijing, China) according to the manufacturer's instructions with the primers listed in supplementary material Table S2. The cells transfected with each mutant were selected by G418.

### Immunoprecipitation

The immunoprecipitation assay was performed as previously reported (Cong et al., 2013). For statistical analysis, the amounts of the same proteins in the input fraction (shown as 'cell lysate') or the reprobated membranes with the immunoprecipitated antibodies were detected as controls.

### Statistical analysis

Data are presented as mean±s.d. Statistical analysis were performed by two-way or one-way ANOVA and followed by Bonferroni's test using GraphPad software (GraphPad Prism 5.0, CA, USA).  $P<0.05$  was considered significant.

### Acknowledgements

We thank Dr David O. Quissell from School of Dentistry, University of Colorado Health Sciences Center, Denver, CO, USA, for the generous gift of the rat SMG-C6 cell line.

### Competing interests

The authors declare no competing or financial interests.

## Author contributions

G.-Y.Y., L.-L.W., X.C. and Y.W. designed the project; X.C., J.L., M.M. and L.-W.Z. performed experiments; Y.Z. and R.-L.X. contributed to statistical analysis; G.-Y.Y., L.-L.W., X.C. and Y.Z. contributed to writing of the manuscript.

## Funding

This study was supported by the National Natural Science Foundation of China [grant numbers 81300893, 81271161, 81470756], and X.C. was supported in part by a Postdoctoral Fellowship from the Peking-Tsinghua Center for Life Sciences.

## Supplementary material

Supplementary material available online at <http://jcs.biologists.org/lookup/suppl/doi:10.1242/jcs.165878/-/DC1>

## References

- Akazawa, Y., Yuki, T., Yoshida, H., Sugiyama, Y. and Inoue, S. (2013). Activation of TRPV4 strengthens the tight-junction barrier in human epidermal keratinocytes. *Skin Pharmacol. Physiol.* **26**, 15–21.
- Anderson, J. M. and Van Itallie, C. M. (2009). Physiology and function of the tight junction. *Cold Spring Harb. Perspect. Biol.* **1**, a002584.
- Aono, S. and Hirai, Y. (2008). Phosphorylation of claudin-4 is required for tight junction formation in a human keratinocyte cell line. *Exp. Cell Res.* **314**, 3326–3339.
- Balda, M. S., González-Mariscal, L., Contreras, R. G., Macías-Silva, M., Torres-Marquez, M. E., García-Sáinz, J. A. and Cerejido, M. (1991). Assembly and sealing of tight junctions: possible participation of G-proteins, phospholipase C, protein kinase C and calmodulin. *J. Membr. Biol.* **122**, 193–202.
- Basuroy, S., Seth, A., Elias, B., Naren, A. P. and Rao, R. (2006). MAPK interacts with occludin and mediates EGF-induced prevention of tight junction disruption by hydrogen peroxide. *Biochem. J.* **393**, 69–77.
- Chattopadhyay, R., Dyukova, E., Singh, N. K., Ohba, M., Mobley, J. A. and Rao, G. N. (2014). Vascular endothelial tight junctions and barrier function are disrupted by 15(S)-hydroxyeicosatetraenoic acid partly via protein kinase C epsilon-mediated zona occludens-1 phosphorylation at threonine 770/772. *J. Biol. Chem.* **289**, 3148–3163.
- Chen, Y.-h., Lu, Q., Schneeberger, E. E. and Goodenough, D. A. (2000). Restoration of tight junction structure and barrier function by down-regulation of the mitogen-activated protein kinase pathway in ras-transformed Madin-Darby canine kidney cells. *Mol. Biol. Cell* **11**, 849–862.
- Cong, X., Zhang, Y., Yang, N.-Y., Li, J., Ding, C., Ding, Q.-W., Su, Y.-C., Mei, M., Guo, X.-H., Wu, L.-L. et al. (2013). Occludin is required for TRPV1-modulated paracellular permeability in the submandibular gland. *J. Cell Sci.* **126**, 1109–1121.
- Coyne, C. B., Vanhook, M. K., Gambling, T. M., Carson, J. L., Boucher, R. C. and Johnson, L. G. (2002). Regulation of airway tight junctions by proinflammatory cytokines. *Mol. Biol. Cell* **13**, 3218–3234.
- Dörfel, M. J. and Huber, O. (2012). Modulation of tight junction structure and function by kinases and phosphatases targeting occludin. *J. Biomed. Biotechnol.* **2012**, 807356.
- D'Souza, T., Agarwal, R. and Morin, P. J. (2005). Phosphorylation of claudin-3 at threonine 192 by cAMP-dependent protein kinase regulates tight junction barrier function in ovarian cancer cells. *J. Biol. Chem.* **280**, 26233–26240.
- D'Souza, T., Indig, F. E. and Morin, P. J. (2007). Phosphorylation of claudin-4 by PKCepsilon regulates tight junction barrier function in ovarian cancer cells. *Exp. Cell Res.* **313**, 3364–3375.
- Ewert, P., Aguilera, S., Allende, C., Kwon, Y.-J., Albornoz, A., Molina, C., Urzúa, U., Quest, A. F. G., Olea, N., Pérez, P. et al. (2010). Disruption of tight junction structure in salivary glands from Sjogren's syndrome patients is linked to proinflammatory cytokine exposure. *Arthritis Rheum.* **62**, 1280–1289.
- Gavard, J. and Gutkind, J. S. (2006). VEGF controls endothelial-cell permeability by promoting the beta-arrestin-dependent endocytosis of VE-cadherin. *Nat. Cell Biol.* **8**, 1223–1234.
- Gong, Y., Yu, M., Yang, J., Gonzales, E., Perez, R., Hou, M., Tripathi, P., Hering-Smith, K. S., Hamm, L. L. and Hou, J. (2014). The Cap1-claudin-4 regulatory pathway is important for renal chloride reabsorption and blood pressure regulation. *Proc. Natl. Acad. Sci. USA* **111**, E3766–E3774.
- González-Mariscal, L., Betanzos, A., Nava, P. and Jaramillo, B. E. (2003). Tight junction proteins. *Prog. Biophys. Mol. Biol.* **81**, 1–44.
- González-Mariscal, L., Tapia, R. and Chamorro, D. (2008). Crosstalk of tight junction components with signaling pathways. *Biochim. Biophys. Acta* **1778**, 729–756.
- Hashimoto, S. and Murakami, M. (2009). Morphological evidence of paracellular transport in perfused rat submandibular glands. *J. Med. Invest.* **56** Suppl., 395–397.
- Hashimoto, S., Murakami, M., Kanaseki, T., Kobayashi, S., Matsuki, M., Shimono, M. and Segawa, A. (2003). Morphological and functional changes in cell junctions during secretory stimulation in the perfused rat submandibular gland. *Eur. J. Morphol.* **41**, 35–39.
- Hopkins, A. M., Walsh, S. V., Verkade, P., Boquet, P. and Nusrat, A. (2003). Constitutive activation of Rho proteins by CNF-1 influences tight junction structure and epithelial barrier function. *J. Cell Sci.* **116**, 725–742.
- Hou, J., Gomes, A. S., Paul, D. L. and Goodenough, D. A. (2006). Study of claudin function by RNA interference. *J. Biol. Chem.* **281**, 36117–36123.
- Ishikawa, Y., Eguchi, T., Skowronski, M. T. and Ishida, H. (1998). Acetylcholine acts on M3 muscarinic receptors and induces the translocation of aquaporin5 water channel via cytosolic Ca<sup>2+</sup> elevation in rat parotid glands. *Biochem. Biophys. Res. Commun.* **245**, 835–840.
- Ivanov, A. I., Nusrat, A. and Parkos, C. A. (2004). Endocytosis of epithelial apical junctional proteins by a clathrin-mediated pathway into a unique storage compartment. *Mol. Biol. Cell* **15**, 176–188.
- Kage, H., Flodby, P., Gao, D., Kim, Y. H., Marconet, C. N., DeMaio, L., Kim, K.-J., Crandall, E. D. and Borok, Z. (2014). Claudin 4 knockout mice: normal physiological phenotype with increased susceptibility to lung injury. *Am. J. Physiol. Lung Cell. Mol. Physiol.* **307**, L524–L536.
- Krause, G., Winkler, L., Mueller, S. L., Haseloff, R. F., Piontek, J. and Blasig, I. E. (2008). Structure and function of claudins. *Biochim. Biophys. Acta* **1778**, 631–645.
- Krupnick, J. G. and Benovic, J. L. (1998). The role of receptor kinases and arrestins in G protein-coupled receptor regulation. *Annu. Rev. Pharmacol. Toxicol.* **38**, 289–319.
- Kumari, S., Mg, S. and Mayor, S. (2010). Endocytosis unplugged: multiple ways to enter the cell. *Cell Res.* **20**, 256–275.
- Lal-Nag, M. and Morin, P. J. (2009). The claudins. *Genome Biol.* **10**, 235.
- Li, D. and Mrsny, R. J. (2000). Oncogenic Raf-1 disrupts epithelial tight junctions via downregulation of occludin. *J. Cell Biol.* **148**, 791–800.
- Lohse, M. J., Benovic, J. L., Codina, J., Caron, M. G. and Lefkowitz, R. J. (1990). beta-Arrestin: a protein that regulates beta-adrenergic receptor function. *Science* **248**, 1547–1550.
- Madara, J. L. (1990). Maintenance of the macromolecular barrier at cell extrusion sites in intestinal epithelium: physiological rearrangement of tight junctions. *J. Membr. Biol.* **116**, 177–184.
- Matsuda, M., Kubo, A., Furuse, M. and Tsukita, S. (2004). A peculiar internalization of claudins, tight junction-specific adhesion molecules, during the intercellular movement of epithelial cells. *J. Cell Sci.* **117**, 1247–1257.
- Melvin, J. E., Yule, D., Shuttleworth, T. and Begenisich, T. (2005). Regulation of fluid and electrolyte secretion in salivary gland acinar cells. *Annu. Rev. Physiol.* **67**, 445–469.
- Merrifield, C. J., Feldman, M. E., Wan, L. and Almers, W. (2002). Imaging actin and dynamin recruitment during invagination of single clathrin-coated pits. *Nat. Cell Biol.* **4**, 691–698.
- Michikawa, H., Fujita-Yoshigaki, J. and Sugiyama, H. (2008). Enhancement of barrier function by overexpression of claudin-4 in tight junctions of submandibular gland cells. *Cell Tissue Res.* **334**, 255–264.
- Min, J. and DeFea, K. (2011). beta-arrestin-dependent actin reorganization: bringing the right players together at the leading edge. *Mol. Pharmacol.* **80**, 760–768.
- Morimoto-Tochigi, A., Walkup, R. D., Nakajima, E., Shearer, T. R. and Azuma, M. (2010). Mechanism for carbachol-induced secretion of lacritin in cultured monkey lacrimal acinar cells. *Invest. Ophthalmol. Vis. Sci.* **51**, 4395–4406.
- Murakami, T., Felinski, E. A. and Antonetti, D. A. (2009). Occludin phosphorylation and ubiquitination regulate tight junction trafficking and vascular endothelial growth factor-induced permeability. *J. Biol. Chem.* **284**, 21036–21046.
- Muza-Moons, M. M., Schneeberger, E. E. and Hecht, G. A. (2004). Enteropathogenic *Escherichia coli* infection leads to appearance of aberrant tight junction strands in the lateral membrane of intestinal epithelial cells. *Cell. Microbiol.* **6**, 783–793.
- Nagaoka, K., Udagawa, T. and Richter, J. D. (2012). CPEB-mediated ZO-1 mRNA localization is required for epithelial tight-junction assembly and cell polarity. *Nat. Commun.* **3**, 675.
- Peerapen, P. and Thongboonkerd, V. (2011). Effects of calcium oxalate monohydrate crystals on expression and function of tight junction of renal tubular epithelial cells. *Lab. Invest.* **91**, 97–105.
- Roth, T. F. and Porter, K. R. (1964). Yolk protein uptake in the oocyte of the mosquito *Aedes Aegypti*. *L. J. Cell Biol.* **20**, 313–332.
- Roxas, J. L., Koutsouris, A., Bellmeyer, A., Tesfay, S., Royan, S., Falzari, K., Harris, A., Cheng, H., Rhee, K. J. and Hecht, G. (2010). Enterohemorrhagic *E. coli* alters murine intestinal epithelial tight junction protein expression and barrier function in a Shiga toxin independent manner. *Lab. Invest.* **90**, 1152–1168.
- Samak, G., Aggarwal, S. and Rao, R. K. (2011). ERK is involved in EGF-mediated protection of tight junctions, but not adherens junctions, in acetaldehyde-treated Caco-2 cell monolayers. *Am. J. Physiol. Gastrointest. Liver Physiol.* **301**, G50–G59.
- Schulzke, J.-D., Günzel, D., John, L. J. and Fromm, M. (2012). Perspectives on tight junction research. *Ann. N. Y. Acad. Sci.* **1257**, 1–19.
- Segawa, A. (1994). Tight junctional permeability in living cells: dynamic changes directly visualized by confocal laser microscopy. *J. Electron Microscop.* **43**, 290–298.

- Sheth, P., Basuroy, S., Li, C., Naren, A. P. and Rao, R. K.** (2003). Role of phosphatidylinositol 3-kinase in oxidative stress-induced disruption of tight junctions. *J. Biol. Chem.* **278**, 49239-49245.
- Shifflett, D. E., Clayburgh, D. R., Koutsouris, A., Turner, J. R. and Hecht, G. A.** (2005). Enteropathogenic *E. coli* disrupts tight junction barrier function and structure in vivo. *Lab. Invest.* **85**, 1308-1324.
- Shrestha, A., Robertson, S. L., Garcia, J., Beingasser, J., McClane, B. A. and Uzal, F. A.** (2014). A synthetic peptide corresponding to the extracellular loop 2 region of claudin-4 protects against clostridium perfringens enterotoxin in vitro and in vivo. *Infect. Immun.* **82**, 4778-4788.
- Shukla, A. K., Kim, J., Ahn, S., Xiao, K., Shenoy, S. K., Liedtke, W. and Lefkowitz, R. J.** (2010). Arresting a transient receptor potential (TRP) channel: beta-arrestin 1 mediates ubiquitination and functional down-regulation of TRPV4. *J. Biol. Chem.* **285**, 30115-30125.
- Simonovic, I., Rosenberg, J., Koutsouris, A. and Hecht, G.** (2000). Enteropathogenic *Escherichia coli* dephosphorylates and dissociates occludin from intestinal epithelial tight junctions. *Cell. Microbiol.* **2**, 305-315.
- Smythe, E. and Ayscough, K. R.** (2006). Actin regulation in endocytosis. *J. Cell Sci.* **119**, 4589-4598.
- Staehein, L. A.** (1973). Further observations on the fine structure of freeze-cleaved tight junctions. *J. Cell Sci.* **13**, 763-786.
- Stevenson, B. R., Anderson, J. M., Braun, I. D. and Mooseker, M. S.** (1989). Phosphorylation of the tight-junction protein ZO-1 in two strains of Madin-Darby canine kidney cells which differ in transepithelial resistance. *Biochem. J.* **263**, 597-599.
- Tsukita, S., Furuse, M. and Itoh, M.** (2001). Multifunctional strands in tight junctions. *Nat. Rev. Mol. Cell Biol.* **2**, 285-293.
- Van Itallie, C., Rahner, C. and Anderson, J. M.** (2001). Regulated expression of claudin-4 decreases paracellular conductance through a selective decrease in sodium permeability. *J. Clin. Invest.* **107**, 1319-1327.
- Wang, F., Graham, W. V., Wang, Y., Witkowski, E. D., Schwarz, B. T. and Turner, J. R.** (2005). Interferon-gamma and tumor necrosis factor-alpha synergize to induce intestinal epithelial barrier dysfunction by up-regulating myosin light chain kinase expression. *Am. J. Pathol.* **166**, 409-419.
- Wood, M. W., Breitschwerdt, E. B., Nordone, S. K., Linder, K. E. and Gookin, J. L.** (2012). Uropathogenic *E. coli* promote a paracellular urothelial barrier defect characterized by altered tight junction integrity, epithelial cell sloughing and cytokine release. *J. Comp. Pathol.* **147**, 11-19.
- Yang, J., Meyer, M., Muller, A.-K., Bohm, F., Grose, R., Dauwalder, T., Verrey, F., Kopf, M., Partanen, J., Bloch, W. et al.** (2010). Fibroblast growth factor receptors 1 and 2 in keratinocytes control the epidermal barrier and cutaneous homeostasis. *J. Cell Biol.* **188**, 935-952.
- Yeh, T.-H., Hsu, L.-W., Tseng, M. T., Lee, P.-L., Sonjae, K., Ho, Y.-C. and Sung, H.-W.** (2011). Mechanism and consequence of chitosan-mediated reversible epithelial tight junction opening. *Biomaterials* **32**, 6164-6173.